Advances in Nano Research, *Vol. 11, No. 5 (2021) 495-519*
https://doi.org/10.12989/anr.2021.11.5.495

Physics-informed neural networks: A deep learning framework for solving the vibrational problems

Xusheng Wang[1], Liang Zhang*[2]

[1]*Xi'an University of Technology, Xi'an 710048, Shaanxi, China*
[2]*School of Aerospace Engineering, Tsinghua University, Beijing 100084, China*

(*Received April 8, 2021, Revised September 26, 2021, Accepted October 5, 2021*)

Abstract. The provided paper considers the vibrations of viscoelastic sandwich disk reinforced by graphene nano-platelets (GPLs) filled viscoelastic concrete (GPLRVC) honeycomb core and face sheets via deep learning. The optimum values of the parameters involved in the fully connected neural network are determined through the momentum-based optimizer. The strength of the method applied in this study comes from the high accuracy besides lower epochs needed to train the multi-layered network. The honeycomb core would be manufactured by aluminum according to its great stiffness and lightweight. The mixture rule and modified Halpin–Tsai model have been involved in creating an efficient concrete material constant. By applying energy methods, the system's governing equations have been extracted and solved through Generalize Differential Quadrature (GDQ) technique. In the given research, Kelvin-Voigt viscoelasticity has been applied to model viscoelastic properties. The time-dependent deflection would be solved applying the fourth-order Runge-Kutta computational approach. Then, a parametric study has been conducted to analyze the influences of the external and internal radius ratio, thickness to length ratio of the concrete, hexagonal core angle, the GPLs' weight fraction, and the honeycomb core's thickness to internal radius ratio on the vibrations of the viscoelastic sandwich disk considering face sheet of FG-GPLRVC and honeycomb core.
Keywords: deep learning, GDQ, honeycomb core, vibrations, viscoelastic sandwich disk,

1. Introduction

Due to the enhancement in applicable structures' thermomechanical response by applying the sandwich system, in the previous decades, scientists discovered a new and decent approach for boosting the low-density shell's dynamics and statics of the, beam, plate, along with disk. This type of system would be employed be in multifarious applications (Gao and Lu 2020, Gao *et al*. 2019, Hu *et al*. 2020). Due to the aforementioned fact, honeycombed systems are provided for use in the pertained industries. Mukhopadhyay and Adhikari (2016) analyzed dynamics of the sandwich panel considering Honeycomb Core employing energy methods. Bourada *et al*. (2020) reported dynamics and stability investigations of SWCNT-filled concrete beam lying on elastic-substrate. Alimirzaei *et al*. (2019) presented nonlinear study of the micro-composite viscoelastic beam with imperfect geometry applying FEM. Many scientists (Draoui *et al*. 2019) provided dynamic and static characteristics of filled sandwich porous plate employing energy approaches (Gao *et al*. 2021a, b, c, Li *et al*. 2021a).

Allam *et al*. (2020) analyzed the natural frequencies of sandwich plates and laminated composite along with shells. They extracted the governing equations employing the refined high-order shear deformation (RHSD) model. The solution procedure in the previous reference can be used for solving complex structures. Refs. (Allam *et al*. 2020) studied the dynamics of FG sandwich plates taking into account the refined shear deformation model. Refs. (Zine *et al*. 2020) analyzed the bending of FG porous plates applying refined shear deformation model. Rabhi *et al*. (2020) analyzed natural frequencies of sandwich plates which was exponentially graded applying a high-order shear deformation model. The decent plate was on an elastic substrate with multifarious boundary conditions (BCs).

Ref. (Suryawanshi *et al*. 2020) analyzed the influences of multifarious defects occurring during the manufacturing of composite honeycomb beams and achieved the honeycomb beams' mechanics in multifarious vibrational modes applying Fast Fourier Transform FE technique and analysis approach. This investigation's significant results disclosed that the structure's frequency drops by raising defect proportion. The lattice core graded corrugated structure's natural frequency and applied an analytical approach for solving the final equations have been evaluated by Ref. (Xu *et al*. 2019). They investigated the influence of graded factors, beam length, and thickness of facial leaf on the mentioned systems' frequency responses. The solution procedure in the previous reference can be used for solving complex structures. Amini *et al*. (2019) studied how to control the vibrations' amplitude of solar panels manufactured by smart layers along with honeycomb core. Employing Hamiltonian and thin plate model, they derived the BCs and motion equations. Ultimately, they found out that elastoelectric influences have a prominent role in the solar panels' vibrations. Ref. (Shahverdi *et al*.

*Corresponding author, Ph.D.,
E-mail: zl19@tsinghua.org.cn

ISSN: 2287-237X (Print), 2287-2388 (Online)

2019) had examined the post-buckling characteristics of panels considering graphene particles reinforcements and honeycomb cores. The scientists' findings illustrate that GPL weight fraction, core thickness, and configurational factors pertained to the panel contribute considerably in the post-buckling characteristics of the sandwich system. The bending analysis of a curved sandwich beam with honeycomb core filled by graphene nanoplatelets layers has been scrutinized by Sobhy (2020). Employing DQM, they solved the complicated motion equations and pertained BCs. Wang *et al*. (2019) carried out a research regarding sandwich system's frequency responses considering honeycomb core applying FE along with empirical outcomes. Ultimately, their vital research discovered that the face-sheet's thickness ratio and its density have a significant role in the sandwich panel's frequency considering a honeycomb core.

Ref. (Zhang *et al*. 2017) reported results of a project regarding a frequency investigation of a sandwich beam considering honeycomb hybrid core applying an FE model and experimental approaches. sandwich honeycomb shell's nonlinear frequency responses had been reported by Zhang and Li (2019). They, however, solved the system's governing equations of the considering simply supported BCs through using the Homotopy perturbation technique. A wide range of scientists worked on the vibrational characteristics of the nano-scaled systems due to Eringen's model as Refs. (Khosravi and Hosseini 2020, Khosravi *et al*. 2020). According to some benefits of GPLs, this type of fillers has got a lot of attention in the previous years. GPLRC plates' natural frequency analysis employing a computational solution process has been reported by Gunasekaran *et al*. (2020). Employing FEM, GPLRC curved plate's forced vibrations subjected to an extremely high-temperature condition has been provided by Ref. (Tran *et al*. 2020). One of the prominent outcomes that they disclosed in their research was that the GPLs' configurational properties have a vital impact on the GPLRC curved plates' resonance behavior. In recent years, the a annular GPLRC sector plates' crucial temperature applying nonlinearity of von Kármán and FOSD model has been reported by Javani *et al*. (2020). The GDQ approach has been employed to solve the final equations, and then they disclosed that by taking into account a few GPLs into the matrix, the crucial temperature would be raised. It is disclosed that annular plates would be employed in multifarious engineering and industrial applications (Mou *et al*. 2020). According to different dynamic and static loads which are able to drop the system's stability, the given system is usually subjected to various conditions (Han, *et al*. 2019). Then, undesirable characteristics are likely to happen for these systems, such as buckling, cracks, deformations, and resonance. Thereby, it would be necessary to imply that the designers have to consider mechanical characteristics of this type of system for investigating the mentioned structure considering the desirable reliability. Due to the GPLs' advantages, this type of material may be employed as a composite filler in the annular plates. The annular GPLRC plates' bending and frequency behaviors applying 3D-elasticity model were evaluated by Liu *et al*. (2019). They solved the the systems' ultimate equations considering the state-space DQ approach. They revealed that a broad range of BCs and other configurational and physical elements of system and GPLs contribute significantly to the bending and frequency characteristics of the annular GPLRC plate. Wang *et al*. (2019) analyzed the thermally impacted annular GPLRC plates' frequency analysis employing GDQ approach. They revealed that multifarious thermal distribution along with locating more square-shaped GPLs may be boosted the dynamics of the annular GPLRC plate in a thermal condition. Safarpour *et al*. (2017a) analyzed viscoelastic annular GPLRC plates' frequency analysis for the first time. They, however, employed GDQM and HSDT for solving and modeling the achieved governing equations, respectively. One of the essential outcomes would be that the viscoelastic factor contributes significantly in the vibrations of a viscoelastic annular GPLRC plate, that this prominent outcome had been achieved employing fourth-order Runge-Kutta computational approach. Annular GPLRC plates' nonlinear forced vibration investigation high-temperature conditions had been introduced by Ref. (Wu *et al*.2020). Applying GDQ approach and iterative technique, they were able to solved the nonlinear final equations and obtained the pertained BCs. Ultimately, they disclosed that the nonlinear frequency ratio drops while more GPLs have been considered into the annular GPLRC plate's external layers. Due to the never-ending attitude of the researchers for analysis of the various systems, GPLs as reinforcement can be used for improving the stability of various structures (Gong *et al*. 2019, Li *et al*. 2019, Zhang *et al*. 2017, 2018).

Due to the extremely detailed analysis in the published papers, no one would be able to assert there could be existed any analysis on the frequency investigation of the viscoelastic sandwich disk considering GPLRVC face sheets and honeycomb core with concrete matrix via deep learning. The optimum values of the parameters involved in the fully connected neural network are determined through the momentum-based optimizer (Cai *et al*. 2021a, b, c, 2020). The strength of the method applied in this study comes from the high accuracy besides lower epochs needed to train the multi-layered network. FSDT has been applied to calculate the relation of stresses-strains. The mixture Rule and modified Halpin–Tsai theory are involved in creating GPLRVC disks' efficient material constant. By applying the Hamiltonian, the structures' governing equations would be achieved. Then, a parametric study is conducted to analyze the influences of the external and internal radius ratio, thickness to length ratio of the concrete, hexagonal core angle, the GPLs' weight fraction, and the honeycomb core's thickness to internal radius ratio on the vibrations of the viscoelastic sandwich disk considering face sheet of FG-GPLRVC and honeycomb core.

2. Mathematical modeling

In the current paper, we analyzed vibrations of a sandwich

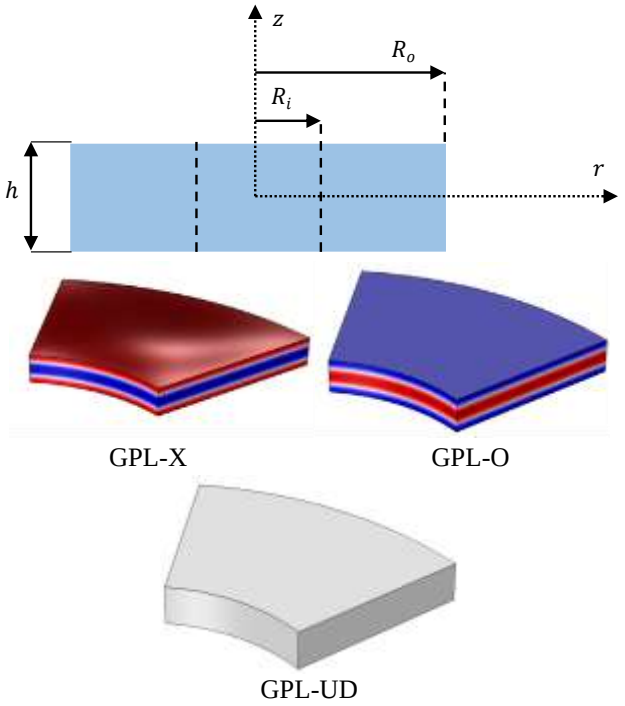

Fig. 1 A disk's configuration covered by the viscoelastic substrate

viscoelastic disk considering honeycomb core GPLRVC face sheets and concrete matrix, as is illustrated in Fig. 1. Moreover, it would be obvious that in the manufacturing procedure, the systems would face with residual stress, so, in the provided calculational technique, we considered internal pressure as residual stress in the sandwich disk. Then, the mathematical formulations of the mentioned problem would be provided in the next step.

Due to the Halpin-Tsai approach, have

$$\bar{E} = -\frac{3}{8}\frac{1+\xi_L\eta_L V_{GPL}}{\eta_L V_{GPL}-1}\times E_M - \frac{5}{8}\frac{1+\xi_W\eta_W V_{GPL}}{\eta_W V_{GPL}-1}\times E_M$$
$$\xi_L = 2\frac{L_{GPL}}{t_{GPL}},\ \xi_W = 2\frac{W_{GPL}}{t_{GPL}},\ \mathrm{V}^*_{GPL} = \frac{\Lambda_{GPL}}{\left(\frac{\rho_{GPL}}{\rho_M}\right)(1-\Lambda_{GPL})+\Lambda_{GPL}} \quad (1)$$
$$\eta_W = -\frac{1-\left(\frac{E_{GPL}}{E_M}\right)}{\xi_W+\left(\frac{E_{GPL}}{E_M}\right)}, \eta_L = \frac{\left(\frac{E_{GPL}}{E_M}\right)-1}{\left(\frac{E_{GPL}}{E_M}\right)+\xi_L}$$

An efficient mass density and Poisson's ratio based on mixture role may be computed as follow

$$\bar{\rho} = \rho_{GPL}V_{GPL} + \rho_M(1-V_{GPL}),\ \bar{\nu} = \nu_{GPL}V_{GPL} + \nu_M(1-V_{GPL}) \quad (2)$$

Then, for efficient shear modulus have

$$\bar{G} = \frac{E_C}{2(1+\nu_C)} \quad (3)$$

Ultimately, various types of GPL distribution through thickness orientation would be provided as next (Ansari and Torabi 2019):

$$V_{GPL}(z_j) = \begin{cases} 2V^*_{GPL}\dfrac{2|z_j|}{h} & \mathrm{GPL}-X \\ 2V^*_{GPL}\left(1-2\dfrac{|z_j|}{h}\right) & \mathrm{GPL}-O \\ V^*_{GPL} & \mathrm{GPL}-UD \end{cases} \quad (4)$$
$$z_j = \left(\frac{1}{2}+\frac{1}{2n}-\frac{j}{n}\right)h, \quad j = 1,2,3,\dots,n$$

2.1 Honeycomb core modelling

The hexagonal cell schematic has been applied in this research. Based on the Gibson model, have (Ebrahimi *et al*. 2018, Esmailpoor Hajilak *et al*. 2019, Ghabussi *et al*. 2019, Gibson and Ashby 1999, Habibi *et al*. 2016, Safarpour *et al*. 2020a, Shariati *et al*. 2020):

$$E^*_{11} = \frac{\sigma_1}{\varepsilon_1} = E_S\left(\frac{t_m}{l_m}\right)\frac{cos(\theta)}{\left(\frac{h_m}{l_m}+sin(\theta)\right)sin^2(\theta)}\frac{1}{1+\left(\frac{t_m}{l_m}\right)^2 cot^2(\theta)} \quad (5a)$$

$$E^*_{22} = \frac{\sigma_2}{\varepsilon_2} = E_S\left(\frac{t_m}{l_m}\right)^3\frac{\left(\frac{h_m}{l_m}+sin(\theta)\right)}{cos^3(\theta)}\frac{1}{1+\left(\frac{t_m}{l_m}\right)^2 cot^2(\theta)} \quad (5b)$$

$$\nu^*_{12} = -\frac{\varepsilon_2}{\varepsilon_1} = \frac{cos^2(\theta)}{\left(\frac{h_m}{l_m+sin(\theta)}\right)sin(\theta)}\frac{1-\left(\frac{t_m}{l_m}\right)^2}{1+cot^2(\theta)\left(\frac{t_m}{l_m}\right)^2} \quad (5c)$$

$$\nu^*_{21} = -\frac{\varepsilon_1}{\varepsilon_2} = \frac{\left(\frac{h_m}{l_m+sin(\theta)}\right)sin(\theta)}{cos^2(\theta)}\frac{1-\left(\frac{t_m}{l_m}\right)^2}{1+\left(\left(\frac{h_m}{l_m}\right)sec^2(\theta)+tan^2(\theta)\right)\left(\frac{t_m}{l_m}\right)^2} \quad (5d)$$

$$G^*_{12} = E_S\left(\frac{t_m}{l_m}\right)^3\frac{\left(\frac{h_m}{l_m+sin(\theta)}\right)}{\left(\frac{h_m}{l_m}\right)^2 cos(\theta)}\frac{1}{\Upsilon} \quad (5e)$$

$$\Upsilon = \begin{pmatrix} 2\dfrac{h_m}{l_m}+1+\dfrac{\frac{h_m}{l_m+sin(\theta)}\left(\frac{t_m}{l_m}\right)^2}{\left(\frac{h_m}{l_m}\right)^2} \\ \left[\left(\frac{h_m}{l_m}+sin(\theta)\right)tan^2(\theta)+sin(\theta)\right] \end{pmatrix} \quad (5f)$$

$$\frac{\rho^*}{\rho_S} = \frac{\left(\frac{t_m}{l_m}\right)\left(\frac{h_m}{l_m}+2\right)}{2\,cos(\theta)\left(\frac{h_m}{l_m}+sin(\theta)\right)} \quad (5g)$$

According to the first-order shear deformation (FSD) model, the fields of displacement would be explained by the next equation (Reddy 2003):

$$u^\eta = {u_0}^\eta + z{u_1}^\eta$$
$$v^\eta = {v_0}^\eta + z{v_1}^\eta \quad (6)$$
$$w^\eta = {w_0}^\eta$$

In the aforementioned relation η explains the bottom, top, and core layers.

2.2 Honeycomb core's stress-strain relations

Applying the Kelvin-Voigt theory, stress-strain equations would be given as next (Habibi *et al*. 2018, 2019b, d, e, Moayedi *et al*. 2020b, Pourjabari *et al*. 2019, Safarpour *et al*. 2019a, Shokrgozar *et al*. 2020):

$$\begin{bmatrix}\sigma_{rr}\\ \sigma_{\theta\theta}\\ \tau_{\theta z}\\ \tau_{rz}\\ \tau_{r\theta}\end{bmatrix}^{c}=\left(1+\tau_s\frac{\partial}{\partial t}\right)\begin{bmatrix}Q_{11} & Q_{12} & 0 & 0 & 0\\ Q_{12} & Q_{22} & 0 & 0 & 0\\ 0 & 0 & Q_{44} & 0 & 0\\ 0 & 0 & 0 & Q_{55} & 0\\ 0 & 0 & 0 & 0 & Q_{66}\end{bmatrix}^{c}\begin{bmatrix}\varepsilon_{rr}\\ \varepsilon_{\theta\theta}\\ \varepsilon_{\theta z}\\ \varepsilon_{rz}\\ \varepsilon_{r\theta}\end{bmatrix}^{c} \tag{7}$$

$$Q_{11}{}^{c}=\frac{E_{11}^{*}}{1-\nu_{12}^{*}\nu_{21}^{*}},$$
$$Q_{22}{}^{c}=\frac{E_{22}^{*}}{1-\nu_{12}^{*}\nu_{21}^{*}}, Q_{12}{}^{c}=\frac{\nu_{21}^{*}E_{22}^{*}}{1-\nu_{12}^{*}\nu_{21}^{*}},$$
$$Q_{44}{}^{c}=G_{12}^{*}, Q_{55}{}^{c}=G_{13}^{*}, Q_{66}{}^{c}=G_{23}^{*}, G_{13}^{*}=G_{23}^{*}=G_{12}^{*}$$

Thereby, the strain elements may be provided as (Al-Furjan *et al*. 2020, Alipour *et al*. 2020, Ebrahimi *et al*. 2020a, Ghabussi *et al*. 2020, Habibi *et al*. 2019a, Safarpour *et al*. 2019b):

$$\begin{Bmatrix}\varepsilon_{RR}\\ \varepsilon_{\theta\theta}\\ \gamma_{R\theta}\\ \gamma_{Rz}\\ \gamma_{\theta z}\end{Bmatrix}^{c}=\begin{bmatrix}\dfrac{\partial u}{\partial R}\\ \dfrac{\partial v}{R\partial\theta}+\dfrac{u}{R}\\ \dfrac{\partial v}{\partial R}+\dfrac{1}{R}\dfrac{\partial u}{\partial\theta}-\dfrac{1}{R}v\\ \dfrac{\partial u}{\partial z}+\dfrac{\partial w}{\partial R}\\ \dfrac{\partial v}{\partial z}+\dfrac{1}{R}\dfrac{\partial w}{\partial\theta}\end{bmatrix}^{c} \tag{8}$$

The face sheet layers' stress-strain equations are as follow (Ghavanloo and Fazelzadeh 2011):

$$\begin{bmatrix}\sigma_{rr}\\ \sigma_{\theta\theta}\\ \tau_{\theta z}\\ \tau_{rz}\\ \tau_{r\theta}\end{bmatrix}^{\psi}=\left(1+\tau_s\frac{\partial}{\partial t}\right)\begin{bmatrix}Q_{11} & Q_{12} & 0 & 0 & 0\\ Q_{12} & Q_{22} & 0 & 0 & 0\\ 0 & 0 & Q_{44} & 0 & 0\\ 0 & 0 & 0 & Q_{55} & 0\\ 0 & 0 & 0 & 0 & Q_{66}\end{bmatrix}^{\psi}\begin{bmatrix}\varepsilon_{rr}\\ \varepsilon_{\theta\theta}\\ \varepsilon_{\theta z}\\ \varepsilon_{rz}\\ \varepsilon_{r\theta}\end{bmatrix}^{\psi} \tag{9}$$

$$Q_{22}{}^{\psi}=Q_{11}{}^{\psi}=\frac{E}{-\nu^2+1}, Q_{12}{}^{\psi}=\frac{E\nu}{-\nu^2+1}, Q_{55}=Q_{44}{}^{\psi}=Q_{66}=G_{12}$$

The relation implied above ψ would define the layers of bottom and top. Thereby, the strain elements could be given as

$$\begin{Bmatrix}\varepsilon_{RR}\\ \varepsilon_{\theta\theta}\\ \gamma_{R\theta}\\ \gamma_{Rz}\\ \gamma_{\theta z}\end{Bmatrix}^{\psi}=\begin{bmatrix}\dfrac{\partial u}{\partial R}\\ \dfrac{\partial v}{\partial\theta R}+\dfrac{u}{R}\\ \dfrac{\partial v}{\partial R}+\dfrac{\partial u}{\partial\theta}\dfrac{1}{R}-\dfrac{v}{R}\\ \dfrac{\partial u}{\partial z}+\dfrac{\partial w}{\partial R}\\ \dfrac{\partial v}{\partial z}+\dfrac{\partial w}{R\partial\theta}\end{bmatrix}^{\psi} \tag{10}$$

2.3 Equations of compatibility

The compatibility conditions taking into account perfect bonding between the composite core and layers which would be able to be defined as

$$\begin{aligned}&u^c(z=-h_c/2)=u^b(z=-h_c/2),\\ &v^c(z=-h_c/2)=v^b(z=-h_c/2),\\ &w^c(z=-h_c/2)=w^b(z=-h_c/2),\\ &u^c(z=h_c/2)=u^t(z=h_c/2),\\ &v^c(z=h_c/2)=v^t(z=h_c/2),\\ &w^c(z=h_c/2)=w^t(z=h_c/2).\end{aligned} \tag{11}$$

2.4 Extended Hamilton's principle:

According to the Energy techniques called the Hamiltonian, there are equations between BCs and motion relations which would be provided as (Ghazanfari *et al*. 2020, Habibi *et al*. 2017, 2019c, Jermsittiparsert *et al*. 2020, Safarpour *et al*. 2018, 2020a):

$$\int_{t_1}^{t_2}\left(\delta T^{*}-\delta U^{*}+\delta W^{*}\right)^{\eta}\,dt=0 \tag{12}$$

The pertained spinning system's kinetic energy could be written as (Ebrahimi *et al*. 2019b, c, 2020b, Habibi *et al*. 2020, Mohammadgholiha *et al*. 2019, Mohammadi *et al*. 2019, Shariati *et al*. 2020, Shokrgozar *et al*. 2020):

$$T^{*\eta}=\int_V\frac{1}{2}\rho^{\eta}\left[\left(\frac{\partial u}{\partial t}\right)^2+\left(\frac{\partial v}{\partial t}\right)^2+\left(\frac{\partial w}{\partial t}\right)^2\right]^{\eta}dV \tag{13a}$$

$$\delta T^{*\eta}=\int_V\rho^{\eta}\left(\frac{\partial u}{\partial t}\frac{\partial\delta u}{\partial t}+\frac{\partial v}{\partial t}\frac{\partial\delta v}{\partial t}+\frac{\partial w}{\partial t}\frac{\partial\delta w}{\partial t}\right)^{\eta}dV \tag{13b}$$

where (Habibi *et al*. 2021, He *et al*. 2021, Huang *et al*. 2021a, Huo *et al*. 2021, Liu *et al*. 2020c, 2021a, Zhang *et al*. 2021c):

$$\{I_0,I_1,I_2\}^{\eta}=\int_{-\frac{h}{2}}^{\frac{h}{2}}\rho^{\eta}\{1,z,z^2\}dZ \tag{14}$$

Then, the given composite's strain energy may be achieved as (Dai *et al*. 2021, Guo *et al*. 2021, Liu *et al*. 2020b, Peng *et al*. 2021, Shao *et al*. 2021, Wang *et al*. 2020b, Wu and Habibi 2021, Zhou *et al*. 2020):

$$\delta U^{*\eta}=\frac{1}{2}\iiint_V\sigma_{ij}^{\eta}\delta\varepsilon_{ij}^{\eta}dV \tag{15}$$

Moreover, the work variation which is conducted by external loads could be achieved as (Hashemi *et al*. 2019, Moayedi *et al*. 2019, 2020a, c, Oyarhossein *et al*. 2020, Shariati *et al*. 2020)

$$\delta W^{*\eta}=\int_A P\left(\frac{1}{r}\frac{\partial w_0}{\partial r}+\frac{\partial^2 w_0}{\partial r^2}+\frac{1}{r^2}\frac{\partial^2 w_0}{\partial\theta^2}\right)dA \tag{16}$$

In which, *P* would be top layer load.

By substitution of Eqs. (13b), (15), and (16) into Eq. (12), after a mathematical manipulation we get the following equations

$$\delta u_{1t}: \frac{M_{rrt}(r,\theta)+r\left(\frac{\partial}{\partial r}M_{rrt}(r,\theta)\right)}{r}-\frac{M_{\theta\theta t}(r,\theta)}{r}+\frac{\frac{\partial}{\partial\theta}M_{r\theta t}(r,\theta)}{r}-N_{rzt}(r,\theta)=\mathrm{K}_{0t}\frac{\partial^2 u_{0c}}{\partial t^2}+\mathrm{K}_{1t}\frac{\partial^2 u_{1c}}{\partial t^2}+\mathrm{K}_{2t}\frac{\partial^2 u_{1t}}{\partial t^2}, \tag{17a}$$

$$\delta v_{1t}: \frac{\frac{\partial}{\partial\theta}M_{\theta\theta t}(r,\theta)}{r}+\frac{M_{r\theta t}(r,\theta)+r\left(\frac{\partial}{\partial r}M_{r\theta t}(r,\theta)\right)}{r}+\frac{M_{r\theta t}(r,\theta)}{r}-N_{\theta zt}(r,\theta)=\mathrm{K}_{0t}\frac{\partial^2 v_{0c}}{\partial t^2}+\mathrm{K}_{1t}\frac{\partial^2 v_{1c}}{\partial t^2}+\mathrm{K}_{2t}\frac{\partial^2 v_{1t}}{\partial t^2}, \tag{17b}$$

$$\begin{gathered}\delta u_{0c}: \frac{N_{rrt}(r,\theta)+r\left(\frac{\partial}{\partial r}N_{rrt}(r,\theta)\right)}{r}-\frac{N_{\theta\theta t}(r,\theta)}{r}+\frac{\frac{\partial}{\partial\theta}N_{r\theta t}(r,\theta)}{r}+\frac{N_{rrc}(r,\theta)+r\left(\frac{\partial}{\partial r}N_{rrc}(r,\theta)\right)}{r}-\frac{N_{\theta\theta c}(r,\theta)}{r}+\frac{\frac{\partial}{\partial\theta}N_{r\theta c}(r,\theta)}{r}+\\ \frac{N_{rrb}(r,\theta)+r\left(\frac{\partial}{\partial r}N_{rrb}(r,\theta)\right)}{r}-\frac{N_{\theta\theta b}(r,\theta)}{r}+\frac{\frac{\partial}{\partial\theta}N_{r\theta b}(r,\theta)}{r}=\mathrm{I}_{0t}\frac{\partial^2 u_{0c}}{\partial t^2}+\mathrm{I}_{1t}\frac{\partial^2 u_{1c}}{\partial t^2}+\mathrm{I}_{2t}\frac{\partial^2 u_{1t}}{\partial t^2}+\mathrm{I}_{0b}\frac{\partial^2 u_{0c}}{\partial t^2}-\mathrm{I}_{1b}\frac{\partial^2 u_{1c}}{\partial t^2}+\\ \mathrm{I}_{2b}\frac{\partial^2 u_{1b}}{\partial t^2}+\mathrm{I}_{0c}\frac{\partial^2 u_{0c}}{\partial t^2}+\mathrm{I}_{1c}\frac{\partial^2 u_{1c}}{\partial t^2},\end{gathered} \tag{17c}$$

$$\begin{gathered}\delta v_{0c}: \frac{\frac{\partial}{\partial\theta}N_{\theta\theta t}(r,\theta)}{r}+\frac{N_{r\theta t}(r,\theta)+r\left(\frac{\partial}{\partial r}N_{r\theta t}(r,\theta)\right)}{r}+\frac{N_{r\theta t}(r,\theta)}{r}+\frac{\frac{\partial}{\partial\theta}N_{\theta\theta c}(r,\theta)}{r}+\frac{N_{r\theta c}(r,\theta)+r\left(\frac{\partial}{\partial r}N_{r\theta c}(r,\theta)\right)}{r}+\frac{N_{r\theta c}(r,\theta)}{r}+\\ \frac{\frac{\partial}{\partial\theta}N_{\theta\theta b}(r,\theta)}{r}+\frac{N_{r\theta b}(r,\theta)+r\left(\frac{\partial}{\partial r}N_{r\theta b}(r,\theta)\right)}{r}+\frac{N_{r\theta b}(r,\theta)}{r}=\mathrm{I}_{0t}\frac{\partial^2 v_{0c}}{\partial t^2}+\mathrm{I}_{1t}\frac{\partial^2 v_{1c}}{\partial t^2}+\mathrm{I}_{2t}\frac{\partial^2 v_{1t}}{\partial t^2}+\mathrm{I}_{0b}\frac{\partial^2 v_{0c}}{\partial t^2}-\mathrm{I}_{1b}\frac{\partial^2 v_{1c}}{\partial t^2}+\\ \mathrm{I}_{2b}\frac{\partial^2 v_{1b}}{\partial t^2}+\mathrm{I}_{0c}\frac{\partial^2 v_{0c}}{\partial t^2}+\mathrm{I}_{1c}\frac{\partial^2 v_{1c}}{\partial t^2},\end{gathered} \tag{17d}$$

$$\begin{gathered}\delta w_{0c}: \frac{N_{rzt}(r,\theta)+r\left(\frac{\partial}{\partial r}N_{rzt}(r,\theta)\right)}{r}+\frac{\frac{\partial}{\partial\theta}N_{\theta zt}(r,\theta)}{r}+\frac{N_{rzc}(r,\theta)+r\left(\frac{\partial}{\partial r}N_{rzc}(r,\theta)\right)}{r}+\frac{\frac{\partial}{\partial\theta}N_{\theta zc}(r,\theta)}{r}+\frac{N_{rzb}(r,\theta)+r\left(\frac{\partial}{\partial r}N_{rzb}(r,\theta)\right)}{r}+\\ \frac{\frac{\partial}{\partial\theta}N_{\theta zb}(r,\theta)}{r}-\mathrm{P}\left(\frac{1}{r}\frac{\partial w_{0c}}{\partial r}+\frac{\partial^2 w_{0c}}{\partial r^2}+\frac{1}{r^2}\frac{\partial^2 w_{0c}}{\partial\theta^2}\right)=\mathrm{I}_{0t}\frac{\partial^2 w_{0c}}{\partial t^2}+\mathrm{I}_{0c}\frac{\partial^2 w_{0c}}{\partial t^2}+\mathrm{I}_{0t}\frac{\partial^2 w_{0c}}{\partial t^2},\end{gathered} \tag{17e}$$

$$\begin{gathered}\delta u_{1c}: \frac{h_c\left(N_{rrt}(r,\theta)+r\left(\frac{\partial}{\partial r}N_{rrt}(r,\theta)\right)\right)}{2r}-\frac{h_c N_{\theta\theta t}(r,\theta)}{2r}+\frac{h_c\left(\frac{\partial}{\partial\theta}N_{r\theta t}(r,\theta)\right)}{2r}+\frac{M_{rrc}(r,\theta)+r\left(\frac{\partial}{\partial r}M_{rrc}(r,\theta)\right)}{r}-\frac{M_{\theta\theta c}(r,\theta)}{r}+\\ \frac{\frac{\partial}{\partial\theta}M_{r\theta c}(r,\theta)}{r}-N_{rzc}(r,\theta)-\frac{h_c\left(N_{rrb}(r,\theta)+r\left(\frac{\partial}{\partial r}N_{rrb}(r,\theta)\right)\right)}{2r}+\frac{h_c N_{\theta\theta b}(r,\theta)}{2r}-\frac{h_c\left(\frac{\partial}{\partial\theta}N_{r\theta b}(r,\theta)\right)}{2r}=\mathrm{J}_{0t}\frac{\partial^2 u_{0c}}{\partial t^2}+\mathrm{J}_{1t}\frac{\partial^2 u_{1c}}{\partial t^2}+\\ \mathrm{J}_{2t}\frac{\partial^2 u_{1t}}{\partial t^2}-\mathrm{J}_{0b}\frac{\partial^2 u_{0c}}{\partial t^2}+\mathrm{J}_{1b}\frac{\partial^2 u_{1c}}{\partial t^2}-\mathrm{J}_{2b}\frac{\partial^2 u_{1b}}{\partial t^2}+\mathrm{I}_{1c}\frac{\partial^2 u_{0c}}{\partial t^2}+\mathrm{I}_{2c}\frac{\partial^2 u_{1c}}{\partial t^2},\end{gathered} \tag{17f}$$

$$\begin{gathered}\delta v_{1c}: \frac{h_c\left(\frac{\partial}{\partial\theta}N_{\theta\theta t}(r,\theta)\right)}{2r}+\frac{h_c\left(N_{r\theta t}(r,\theta)+r\left(\frac{\partial}{\partial r}N_{r\theta t}(r,\theta)\right)\right)}{2r}+\frac{h_c N_{r\theta t}(r,\theta)}{2r}+\frac{\frac{\partial}{\partial\theta}M_{\theta\theta c}(r,\theta)}{r}+\frac{M_{r\theta c}(r,\theta)+r\left(\frac{\partial}{\partial r}M_{r\theta c}(r,\theta)\right)}{r}+\\ \frac{M_{r\theta c}(r,\theta)}{r}-N_{\theta zc}(r,\theta)-\frac{h_c\left(\frac{\partial}{\partial\theta}N_{\theta\theta b}(r,\theta)\right)}{2r}-\frac{h_c\left(N_{r\theta b}(r,\theta)+r\left(\frac{\partial}{\partial r}N_{r\theta b}(r,\theta)\right)\right)}{2r}-\frac{h_c N_{r\theta b}(r,\theta)}{2r}=\mathrm{J}_{0t}\frac{\partial^2 v_{0c}}{\partial t^2}+\mathrm{J}_{1t}\frac{\partial^2 v_{1c}}{\partial t^2}+\\ \mathrm{J}_{2t}\frac{\partial^2 v_{1t}}{\partial t^2}-\mathrm{J}_{0b}\frac{\partial^2 v_{0c}}{\partial t^2}+\mathrm{J}_{1b}\frac{\partial^2 v_{1c}}{\partial t^2}-\mathrm{J}_{2b}\frac{\partial^2 v_{1b}}{\partial t^2}+\mathrm{I}_{1c}\frac{\partial^2 v_{0c}}{\partial t^2}+\mathrm{I}_{2c}\frac{\partial^2 v_{1c}}{\partial t^2},\end{gathered} \tag{17g}$$

$$\delta u_{1b}=\frac{M_{rrb}(r,\theta)+r\left(\frac{\partial}{\partial r}M_{rrb}(r,\theta)\right)}{r}-\frac{M_{\theta\theta b}(r,\theta)}{r}+\frac{\frac{\partial}{\partial\theta}M_{r\theta b}(r,\theta)}{r}-N_{rzb}(r,\theta)=\mathrm{K}_{0b}\frac{\partial^2 u_{0c}}{\partial t^2}-\mathrm{K}_{1b}\frac{\partial^2 u_{1c}}{\partial t^2}+\mathrm{K}_{2b}\frac{\partial^2 u_{1b}}{\partial t^2}, \tag{17h}$$

$$\delta v_{1b}: \frac{\frac{\partial}{\partial\theta}M_{\theta\theta b}(r,\theta)}{r}+\frac{M_{r\theta b}(r,\theta)+r\left(\frac{\partial}{\partial r}M_{r\theta b}(r,\theta)\right)}{r}+\frac{M_{r\theta b}(r,\theta)}{r}-N_{\theta zb}(r,\theta)=\mathrm{K}_{0b}\frac{\partial^2 v_{0c}}{\partial t^2}-\mathrm{K}_{1b}\frac{\partial^2 v_{1c}}{\partial t^2}+\mathrm{K}_{2b}\frac{\partial^2 v_{1b}}{\partial t^2}, \tag{17i}$$

In which:

$$\begin{gathered}N_{rrt}=\left(1+\tau_s\frac{\partial}{\partial t}\right)\left(A_{11t}\frac{\partial u_{0c}}{\partial r}+B_{11t}\frac{\partial u_{1t}}{\partial r}+\frac{h_c}{2}A_{11t}\frac{\partial u_{1c}}{\partial r}+A_{12t}\frac{u_{0c}}{r}+B_{12t}\frac{u_{1t}}{r}+\frac{h_c}{2}A_{12t}\frac{u_{1c}}{r}+\frac{A_{12t}}{r}\frac{\partial v_{0c}}{\partial\theta}+\right.\\ \left.\frac{B_{12t}}{r}\frac{\partial v_{1t}}{\partial\theta}+\frac{h_c}{2}\frac{A_{12t}}{r}\frac{\partial v_{1c}}{\partial\theta}\right),\\ M_{rrt}=\left(1+\tau_s\frac{\partial}{\partial t}\right)\left(B_{11t}\frac{\partial u_{0c}}{\partial r}+C_{11t}\frac{\partial u_{1t}}{\partial r}+\frac{h_c}{2}B_{11t}\frac{\partial u_{1c}}{\partial r}+B_{12t}\frac{u_{0c}}{r}+C_{12t}\frac{u_{1t}}{r}+\frac{h_c}{2}B_{12t}\frac{u_{1c}}{r}+\frac{B_{12t}}{r}\frac{\partial v_{0c}}{\partial\theta}+\right.\\ \left.\frac{C_{12t}}{r}\frac{\partial v_{1t}}{\partial\theta}+\frac{h_c}{2}\frac{B_{12t}}{r}\frac{\partial v_{1c}}{\partial\theta}\right),\end{gathered} \tag{18}$$

$$N_{\theta\theta t}=\left(1+\tau_s\frac{\partial}{\partial t}\right)\left(A_{12t}\frac{\partial u_{0c}}{\partial r}+B_{12t}\frac{\partial u_{1t}}{\partial r}+\frac{h_c}{2}A_{12t}\frac{\partial u_{1c}}{\partial r}+A_{22t}\frac{u_{0c}}{r}+B_{22t}\frac{u_{1t}}{r}+\frac{h_c}{2}A_{22t}\frac{u_{1c}}{r}+\frac{A_{22t}}{r}\frac{\partial v_{0c}}{\partial\theta}+\frac{B_{22t}}{r}\frac{\partial v_{1t}}{\partial\theta}+\frac{h_c}{2}\frac{A_{22t}}{r}\frac{\partial v_{1c}}{\partial\theta}\right),$$

$$M_{\theta\theta t}=\left(1+\tau_s\frac{\partial}{\partial t}\right)\left(B_{12t}\frac{\partial u_{0c}}{\partial r}+C_{12t}\frac{\partial u_{1t}}{\partial r}+\frac{h_c}{2}B_{12t}\frac{\partial u_{1c}}{\partial r}+B_{22t}\frac{u_{0c}}{r}+C_{22t}\frac{u_{1t}}{r}+\frac{h_c}{2}B_{22t}\frac{u_{1c}}{r}+\frac{B_{22t}}{r}\frac{\partial v_{0c}}{\partial\theta}+\frac{C_{22t}}{r}\frac{\partial v_{1t}}{\partial\theta}+\frac{h_c}{2}\frac{B_{22t}}{r}\frac{\partial v_{1c}}{\partial\theta}\right),$$

$$N_{\theta zt}=\left(1+\tau_s\frac{\partial}{\partial t}\right)\left(A_{44t}v_{1t}+\frac{A_{44t}}{r}\frac{\partial w_{0c}}{\partial\theta}\right),$$

$$M_{\theta zt}=\left(1+\tau_s\frac{\partial}{\partial t}\right)\left(B_{44t}v_{1t}+\frac{B_{44t}}{r}\frac{\partial w_{0c}}{\partial\theta}\right),$$

$$N_{rzt}=\left(1+\tau_s\frac{\partial}{\partial t}\right)\left(A_{55t}u_{1t}+A_{55t}\frac{\partial w_{0c}}{\partial r}\right),$$

$$M_{rzt}=\left(1+\tau_s\frac{\partial}{\partial t}\right)\left(B_{55t}u_{1t}+B_{55t}\frac{\partial w_{0c}}{\partial r}\right),$$

$$N_{r\theta t}=\left(1+\tau_s\frac{\partial}{\partial t}\right)\left(\frac{A_{66t}\left(\frac{\partial}{\partial\theta}u_{0c}\right)}{r}+\frac{B_{66t}\left(\frac{\partial}{\partial\theta}u_{1t}\right)}{r}+\frac{A_{66t}h_c\left(\frac{\partial}{\partial\theta}u_{1c}\right)}{2r}+A_{66t}\left(\frac{\partial}{\partial r}v_{0c}\right)+B_{66t}\left(\frac{\partial}{\partial r}v_{1t}\right)+\frac{h_cA_{66t}\left(\frac{\partial}{\partial r}v_{1c}\right)}{2}-\frac{A_{66t}v_{0c}}{r}-\frac{B_{66t}v_{1t}}{r}-\frac{A_{66t}h_cv_{1c}}{2r}\right),$$

$$M_{r\theta b}=\left(1+\tau_s\frac{\partial}{\partial t}\right)\left(\frac{B_{66b}\left(\frac{\partial}{\partial\theta}u_{0c}\right)}{r}+\frac{C_{66b}\left(\frac{\partial}{\partial\theta}u_{1b}\right)}{r}-\frac{B_{66b}h_c\left(\frac{\partial}{\partial\theta}u_{1c}\right)}{2r}+B_{66b}\left(\frac{\partial}{\partial r}v_{0c}\right)+C_{66b}\left(\frac{\partial}{\partial r}v_{1t}\right)-\frac{h_cB_{66b}\left(\frac{\partial}{\partial r}v_{1c}\right)}{2}-\frac{B_{66b}v_{0c}}{r}-\frac{C_{66b}v_{1t}}{r}+\frac{B_{66b}h_cv_{1c}}{2r}\right),\tag{18}$$

$$N_{rrc}=\left(1+\tau_s\frac{\partial}{\partial t}\right)\left(A_{11c}\frac{\partial u_{0c}}{\partial r}+B_{11c}\frac{\partial u_{1c}}{\partial r}+A_{12c}\frac{u_{0c}}{r}+B_{12c}\frac{u_{1c}}{r}+\frac{A_{12c}}{r}\frac{\partial v_{0c}}{\partial\theta}+\frac{B_{12c}}{r}\frac{\partial v_{1c}}{\partial\theta}\right),$$

$$M_{rrc}=\left(1+\tau_s\frac{\partial}{\partial t}\right)\left(B_{11c}\frac{\partial u_{0c}}{\partial r}+C_{11c}\frac{\partial u_{1c}}{\partial r}+B_{12c}\frac{u_{0c}}{r}+C_{12c}\frac{u_{1c}}{r}+\frac{B_{12c}}{r}\frac{\partial v_{0c}}{\partial\theta}+\frac{C_{12c}}{r}\frac{\partial v_{1c}}{\partial\theta}\right),$$

$$N_{\theta\theta c}=\left(1+\tau_s\frac{\partial}{\partial t}\right)\left(A_{12c}\frac{\partial u_{0c}}{\partial r}+B_{12c}\frac{\partial u_{1c}}{\partial r}+A_{22c}\frac{u_{0c}}{r}+B_{22c}\frac{u_{1c}}{r}+\frac{A_{22c}}{r}\frac{\partial v_{0c}}{\partial\theta}+\frac{B_{22c}}{r}\frac{\partial v_{1c}}{\partial\theta}\right),$$

$$M_{\theta\theta c}=\left(1+\tau_s\frac{\partial}{\partial t}\right)\left(B_{12c}\frac{\partial u_{0c}}{\partial r}+C_{12c}\frac{\partial u_{1c}}{\partial r}+B_{22c}\frac{u_{0c}}{r}+C_{22c}\frac{u_{1c}}{r}+\frac{B_{22c}}{r}\frac{\partial v_{0c}}{\partial\theta}+\frac{C_{22c}}{r}\frac{\partial v_{1c}}{\partial\theta}\right),$$

$$N_{\theta zc}=\left(1+\tau_s\frac{\partial}{\partial t}\right)\left(A_{44t}v_{1c}+\frac{A_{44c}}{r}\frac{\partial w_{0c}}{\partial\theta}\right),$$

$$M_{\theta zc}=\left(1+\tau_s\frac{\partial}{\partial t}\right)\left(B_{44c}v_{1c}+\frac{B_{44c}}{r}\frac{\partial w_{0c}}{\partial\theta}\right),$$

$$N_{rzc}=\left(1+\tau_s\frac{\partial}{\partial t}\right)\left(A_{55c}u_{1c}+A_{55c}\frac{\partial w_{0c}}{\partial r}\right),$$

$$M_{rzc}=\left(1+\tau_s\frac{\partial}{\partial t}\right)\left(B_{55c}u_{1c}+B_{55c}\frac{\partial w_{0c}}{\partial r}\right),$$

$$N_{r\theta c}=\left(1+\tau_s\frac{\partial}{\partial t}\right)\left(\frac{A_{66c}\left(\frac{\partial}{\partial\theta}u_{0c}\right)}{r}+\frac{B_{66c}\left(\frac{\partial}{\partial\theta}u_{1c}\right)}{r}+A_{66c}\left(\frac{\partial}{\partial r}v_{0c}\right)+B_{66c}\left(\frac{\partial}{\partial r}v_{1t}\right)-\frac{A_{66c}v_{0c}}{r}-\frac{B_{66c}v_{1c}}{r}\right),$$

$$M_{r\theta c}=\left(1+\tau_s\frac{\partial}{\partial t}\right)\left(\frac{B_{66c}\left(\frac{\partial}{\partial\theta}u_{0c}\right)}{r}+\frac{C_{66c}\left(\frac{\partial}{\partial\theta}u_{1c}\right)}{r}+B_{66c}\left(\frac{\partial}{\partial r}v_{0c}\right)+C_{66c}\left(\frac{\partial}{\partial r}v_{1t}\right)-\frac{B_{66c}v_{0c}}{r}-\frac{C_{66c}v_{1c}}{r}\right),$$

By substituting Eq. (18) in to Eq. (17) can be written as follows

$$\delta u_{1t}:\frac{1}{r}\left(\left(\left(1+\tau_s\frac{\partial}{\partial t}\right)\left(B_{11t}\frac{\partial u_{0c}}{\partial r}+C_{11t}\frac{\partial u_{1t}}{\partial r}+\frac{h_c}{2}B_{11t}\frac{\partial u_{1c}}{\partial r}+B_{12t}\frac{u_{0c}}{r}+C_{12t}\frac{u_{1t}}{r}+\frac{h_c}{2}B_{12t}\frac{u_{1c}}{r}+\frac{B_{12t}}{r}\frac{\partial v_{0c}}{\partial \theta}+\frac{C_{12t}}{r}\frac{\partial v_{1t}}{\partial \theta}+\frac{h_c}{2}\frac{B_{12t}}{r}\frac{\partial v_{1c}}{\partial \theta}\right)\right)+r\left(\frac{\partial}{\partial r}\left(\left(1+\tau_s\frac{\partial}{\partial t}\right)\left(B_{11t}\frac{\partial u_{0c}}{\partial r}+C_{11t}\frac{\partial u_{1t}}{\partial r}+\frac{h_c}{2}B_{11t}\frac{\partial u_{1c}}{\partial r}+B_{12t}\frac{u_{0c}}{r}+C_{12t}\frac{u_{1t}}{r}+\frac{h_c}{2}B_{12t}\frac{u_{1c}}{r}+\frac{B_{12t}}{r}\frac{\partial v_{0c}}{\partial \theta}+\frac{C_{12t}}{r}\frac{\partial v_{1t}}{\partial \theta}+\frac{h_c}{2}\frac{B_{12t}}{r}\frac{\partial v_{1c}}{\partial \theta}\right)\right)\right)\right)-\frac{1}{r}\left(\left(1+\tau_s\frac{\partial}{\partial t}\right)\left(B_{12t}\frac{\partial u_{0c}}{\partial r}+C_{12t}\frac{\partial u_{1t}}{\partial r}+\frac{h_c}{2}B_{12t}\frac{\partial u_{1c}}{\partial r}+B_{22t}\frac{u_{0c}}{r}+C_{22t}\frac{u_{1t}}{r}+\frac{h_c}{2}B_{22t}\frac{u_{1c}}{r}+\frac{B_{22t}}{r}\frac{\partial v_{0c}}{\partial \theta}+\frac{C_{22t}}{r}\frac{\partial v_{1t}}{\partial \theta}+\frac{h_c}{2}\frac{B_{22t}}{r}\frac{\partial v_{1c}}{\partial \theta}\right)\right)+\frac{1}{r}\left(\frac{\partial}{\partial \theta}\left(\left(1+\tau_s\frac{\partial}{\partial t}\right)\left(\frac{B_{66t}\left(\frac{\partial}{\partial \theta}u_{0c}\right)}{r}+\frac{C_{66t}\left(\frac{\partial}{\partial \theta}u_{1t}\right)}{r}+\frac{B_{66t}h_c\left(\frac{\partial}{\partial \theta}u_{1c}\right)}{2r}+B_{66t}\left(\frac{\partial}{\partial r}v_{0c}\right)+C_{66t}\left(\frac{\partial}{\partial r}v_{1t}\right)+\frac{h_cB_{66t}\left(\frac{\partial}{\partial r}v_{1c}\right)}{2}-\frac{B_{66t}v_{0c}}{r}-\frac{C_{66t}v_{1t}}{r}-\frac{B_{66t}h_cv_{1c}}{2r}\right)\right)\right)-\left(\left(1+\tau_s\frac{\partial}{\partial t}\right)\left(A_{55t}u_{1t}+A_{55t}\frac{\partial w_{0c}}{\partial r}\right)\right)=\mathrm{K}_{0t}\frac{\partial^2 u_{0c}}{\partial t^2}+\mathrm{K}_{1t}\frac{\partial^2 u_{1c}}{\partial t^2}+\mathrm{K}_{2t}\frac{\partial^2 u_{1t}}{\partial t^2}, \tag{19a}$$

$$\delta v_{1t}:\frac{1}{r}\left(\frac{\partial}{\partial \theta}\left(\left(1+\tau_s\frac{\partial}{\partial t}\right)\left(B_{12t}\frac{\partial u_{0c}}{\partial r}+C_{12t}\frac{\partial u_{1t}}{\partial r}+\frac{h_c}{2}B_{12t}\frac{\partial u_{1c}}{\partial r}+B_{22t}\frac{u_{0c}}{r}+C_{22t}\frac{u_{1t}}{r}+\frac{h_c}{2}B_{22t}\frac{u_{1c}}{r}+\frac{B_{22t}}{r}\frac{\partial v_{0c}}{\partial \theta}+\frac{C_{22t}}{r}\frac{\partial v_{1t}}{\partial \theta}+\frac{h_c}{2}\frac{B_{22t}}{r}\frac{\partial v_{1c}}{\partial \theta}\right)\right)\right)+\frac{1}{r}\left(\left(\left(1+\tau_s\frac{\partial}{\partial t}\right)\left(\frac{B_{66t}\left(\frac{\partial}{\partial \theta}u_{0c}\right)}{r}+\frac{C_{66t}\left(\frac{\partial}{\partial \theta}u_{1t}\right)}{r}+\frac{B_{66t}h_c\left(\frac{\partial}{\partial \theta}u_{1c}\right)}{2r}+B_{66t}\left(\frac{\partial}{\partial r}v_{0c}\right)+C_{66t}\left(\frac{\partial}{\partial r}v_{1t}\right)+\frac{h_cB_{66t}\left(\frac{\partial}{\partial r}v_{1c}\right)}{2}-\frac{B_{66t}v_{0c}}{r}-\frac{C_{66t}v_{1t}}{r}-\frac{B_{66t}h_cv_{1c}}{2r}\right)\right)+r\left(\frac{\partial}{\partial r}\left(\left(1+\tau_s\frac{\partial}{\partial t}\right)\left(\frac{B_{66t}\left(\frac{\partial}{\partial \theta}u_{0c}\right)}{r}+\frac{C_{66t}\left(\frac{\partial}{\partial \theta}u_{1t}\right)}{r}+\frac{B_{66t}h_c\left(\frac{\partial}{\partial \theta}u_{1c}\right)}{2r}+B_{66t}\left(\frac{\partial}{\partial r}v_{0c}\right)+C_{66t}\left(\frac{\partial}{\partial r}v_{1t}\right)+\frac{h_cB_{66t}\left(\frac{\partial}{\partial r}v_{1c}\right)}{2}-\frac{B_{66t}v_{0c}}{r}-\frac{C_{66t}v_{1t}}{r}-\frac{B_{66t}h_cv_{1c}}{2r}\right)\right)\right)\right)+\frac{1}{r}\left(\left(1+\tau_s\frac{\partial}{\partial t}\right)\left(\frac{B_{66t}\left(\frac{\partial}{\partial \theta}u_{0c}\right)}{r}+\frac{C_{66t}\left(\frac{\partial}{\partial \theta}u_{1t}\right)}{r}+\frac{B_{66t}h_c\left(\frac{\partial}{\partial \theta}u_{1c}\right)}{2r}+B_{66t}\left(\frac{\partial}{\partial r}v_{0c}\right)+C_{66t}\left(\frac{\partial}{\partial r}v_{1t}\right)+\frac{h_cB_{66t}\left(\frac{\partial}{\partial r}v_{1c}\right)}{2}-\frac{B_{66t}v_{0c}}{r}-\frac{C_{66t}v_{1t}}{r}-\frac{B_{66t}h_cv_{1c}}{2r}\right)\right)-\left(\left(1+\tau_s\frac{\partial}{\partial t}\right)\left(B_{44t}v_{1t}+\frac{B_{44t}}{r}\frac{\partial w_{0c}}{\partial \theta}\right)\right)=\mathrm{K}_{0t}\frac{\partial^2 v_{0c}}{\partial t^2}+\mathrm{K}_{1t}\frac{\partial^2 v_{1c}}{\partial t^2}+\mathrm{K}_{2t}\frac{\partial^2 v_{1t}}{\partial t^2}, \tag{19b}$$

$$u_{0c}:\frac{1}{r}\left(\left(\left(1+\tau_s\frac{\partial}{\partial t}\right)\left(A_{11t}\frac{\partial u_{0c}}{\partial r}+B_{11t}\frac{\partial u_{1t}}{\partial r}+\frac{h_c}{2}A_{11t}\frac{\partial u_{1c}}{\partial r}+A_{12t}\frac{u_{0c}}{r}+B_{12t}\frac{u_{1t}}{r}+\frac{h_c}{2}A_{12t}\frac{u_{1c}}{r}+\frac{A_{12t}}{r}\frac{\partial v_{0c}}{\partial \theta}+\frac{B_{12t}}{r}\frac{\partial v_{1t}}{\partial \theta}+\frac{h_c}{2}\frac{A_{12t}}{r}\frac{\partial v_{1c}}{\partial \theta}\right)\right)+r\left(\frac{\partial}{\partial r}\left(\left(1+\tau_s\frac{\partial}{\partial t}\right)\left(A_{11t}\frac{\partial u_{0c}}{\partial r}+B_{11t}\frac{\partial u_{1t}}{\partial r}+\frac{h_c}{2}A_{11t}\frac{\partial u_{1c}}{\partial r}+A_{12t}\frac{u_{0c}}{r}+B_{12t}\frac{u_{1t}}{r}+\frac{h_c}{2}A_{12t}\frac{u_{1c}}{r}+\frac{A_{12t}}{r}\frac{\partial v_{0c}}{\partial \theta}+\frac{B_{12t}}{r}\frac{\partial v_{1t}}{\partial \theta}+\frac{h_c}{2}\frac{A_{12t}}{r}\frac{\partial v_{1c}}{\partial \theta}\right)\right)\right)\right)-\frac{1}{r}\left(\left(1+\tau_s\frac{\partial}{\partial t}\right)\left(A_{12t}\frac{\partial u_{0c}}{\partial r}+B_{12t}\frac{\partial u_{1t}}{\partial r}+\frac{h_c}{2}A_{12t}\frac{\partial u_{1c}}{\partial r}+A_{22t}\frac{u_{0c}}{r}+B_{22t}\frac{u_{1t}}{r}+\frac{h_c}{2}A_{22t}\frac{u_{1c}}{r}+\frac{A_{22t}}{r}\frac{\partial v_{0c}}{\partial \theta}+\frac{B_{22t}}{r}\frac{\partial v_{1t}}{\partial \theta}+\frac{h_c}{2}\frac{A_{22t}}{r}\frac{\partial v_{1c}}{\partial \theta}\right)\right) \tag{19c}$$

$$+\frac{1}{r}\left(\frac{\partial}{\partial\theta}\left(\left(1+\tau_s\frac{\partial}{\partial t}\right)\left(\frac{A_{66t}\left(\frac{\partial}{\partial\theta}u_{0c}\right)}{r}+\frac{B_{66t}\left(\frac{\partial}{\partial\theta}u_{1t}\right)}{r}+\frac{A_{66t}h_c\left(\frac{\partial}{\partial\theta}u_{1c}\right)}{2r}+A_{66t}\left(\frac{\partial}{\partial r}v_{0c}\right)+B_{66t}\left(\frac{\partial}{\partial r}v_{1t}\right)+\right.\right.\right.$$

$$\left.\left.\left.\frac{h_cA_{66t}\left(\frac{\partial}{\partial r}v_{1c}\right)}{2}-\frac{A_{66t}v_{0c}}{r}-\frac{B_{66t}v_{1t}}{r}-\frac{A_{66t}h_cv_{1c}}{2r}\right)\right)\right)+\frac{1}{r}\left(\left(\left(1+\tau_s\frac{\partial}{\partial t}\right)\left(A_{11c}\frac{\partial u_{0c}}{\partial r}+B_{11c}\frac{\partial u_{1c}}{\partial r}+A_{12c}\frac{u_{0c}}{r}+\right.\right.\right.$$

$$\left.\left.\left.B_{12c}\frac{u_{1c}}{r}+\frac{A_{12c}}{r}\frac{\partial v_{0c}}{\partial\theta}+\frac{B_{12c}}{r}\frac{\partial v_{1c}}{\partial\theta}\right)\right)+r\left(\frac{\partial}{\partial r}\left(\left(1+\tau_s\frac{\partial}{\partial t}\right)\left(A_{11c}\frac{\partial u_{0c}}{\partial r}+B_{11c}\frac{\partial u_{1c}}{\partial r}+A_{12c}\frac{u_{0c}}{r}+B_{12c}\frac{u_{1c}}{r}+\right.\right.\right.\right.$$

$$\left.\left.\left.\left.\frac{A_{12c}}{r}\frac{\partial v_{0c}}{\partial\theta}+\frac{B_{12c}}{r}\frac{\partial v_{1c}}{\partial\theta}\right)\right)\right)\right)-\frac{1}{r}\left(\left(1+\tau_s\frac{\partial}{\partial t}\right)\left(A_{12c}\frac{\partial u_{0c}}{\partial r}+B_{12c}\frac{\partial u_{1c}}{\partial r}+A_{22c}\frac{u_{0c}}{r}+B_{22c}\frac{u_{1c}}{r}+\frac{A_{22c}}{r}\frac{\partial v_{0c}}{\partial\theta}+\right.\right.$$

$$\left.\left.\frac{B_{22c}}{r}\frac{\partial v_{1c}}{\partial\theta}\right)\right)+\frac{1}{r}\left(\frac{\partial}{\partial\theta}\left(\left(1+\tau_s\frac{\partial}{\partial t}\right)\left(\frac{A_{66c}\left(\frac{\partial}{\partial\theta}u_{0c}\right)}{r}+\frac{B_{66c}\left(\frac{\partial}{\partial\theta}u_{1c}\right)}{r}+A_{66c}\left(\frac{\partial}{\partial r}v_{0c}\right)+B_{66c}\left(\frac{\partial}{\partial r}v_{1t}\right)-\frac{A_{66c}v_{0c}}{r}-\right.\right.\right.$$

$$\left.\left.\left.\frac{B_{66c}v_{1c}}{r}\right)\right)\right)+\frac{1}{r}\left(\left(\left(1+\tau_s\frac{\partial}{\partial t}\right)\left(A_{11b}\frac{\partial u_{0c}}{\partial r}+B_{11b}\frac{\partial u_{1b}}{\partial r}-\frac{h_c}{2}A_{11b}\frac{\partial u_{1c}}{\partial r}+A_{12b}\frac{u_{0c}}{r}+B_{12b}\frac{u_{1t}}{r}-\frac{h_c}{2}A_{12b}\frac{u_{1c}}{r}+\right.\right.\right.\right. \quad (19c)$$

$$\left.\left.\left.\left.\frac{A_{12b}}{r}\frac{\partial v_{0c}}{\partial\theta}+\frac{B_{12b}}{r}\frac{\partial v_{1b}}{\partial\theta}-\frac{h_c}{2}\frac{A_{12b}}{r}\frac{\partial v_{1c}}{\partial\theta}\right)\right)+r\left(\frac{\partial}{\partial r}\left(\left(1+\tau_s\frac{\partial}{\partial t}\right)\left(A_{11b}\frac{\partial u_{0c}}{\partial r}+B_{11b}\frac{\partial u_{1b}}{\partial r}-\frac{h_c}{2}A_{11b}\frac{\partial u_{1c}}{\partial r}+A_{12b}\frac{u_{0c}}{r}+\right.\right.\right.\right.\right.$$

$$\left.\left.\left.\left.\left.B_{12b}\frac{u_{1t}}{r}-\frac{h_c}{2}A_{12b}\frac{u_{1c}}{r}+\frac{A_{12b}}{r}\frac{\partial v_{0c}}{\partial\theta}+\frac{B_{12b}}{r}\frac{\partial v_{1b}}{\partial\theta}-\frac{h_c}{2}\frac{A_{12b}}{r}\frac{\partial v_{1c}}{\partial\theta}\right)\right)\right)\right)-\frac{1}{r}\left(\left(1+\tau_s\frac{\partial}{\partial t}\right)\left(A_{12b}\frac{\partial u_{0c}}{\partial r}+B_{12b}\frac{\partial u_{1b}}{\partial r}-\right.\right.$$

$$\left.\left.\frac{h_c}{2}A_{12b}\frac{\partial u_{1c}}{\partial r}+A_{22b}\frac{u_{0c}}{r}+B_{22b}\frac{u_{1t}}{r}-\frac{h_c}{2}A_{22b}\frac{u_{1c}}{r}+\frac{A_{22b}}{r}\frac{\partial v_{0c}}{\partial\theta}+\frac{B_{22b}}{r}\frac{\partial v_{1b}}{\partial\theta}-\frac{h_c}{2}\frac{A_{22b}}{r}\frac{\partial v_{1c}}{\partial\theta}\right)\right)+\frac{1}{r}\left(\frac{\partial}{\partial\theta}\left(\left(1+\right.\right.\right.$$

$$\left.\left.\left.\tau_s\frac{\partial}{\partial t}\right)\left(\frac{A_{66b}\left(\frac{\partial}{\partial\theta}u_{0c}\right)}{r}+\frac{B_{66b}\left(\frac{\partial}{\partial\theta}u_{1b}\right)}{r}-\frac{A_{66b}h_c\left(\frac{\partial}{\partial\theta}u_{1c}\right)}{2r}+A_{66b}\left(\frac{\partial}{\partial r}v_{0c}\right)+B_{66b}\left(\frac{\partial}{\partial r}v_{1t}\right)-\frac{h_cA_{66b}\left(\frac{\partial}{\partial r}v_{1c}\right)}{2}-\frac{A_{66b}v_{0c}}{r}-\right.\right.\right.$$

$$\left.\left.\left.\frac{B_{66b}v_{1t}}{r}+\frac{A_{66b}h_cv_{1c}}{2r}\right)\right)\right)=\mathrm{I}_{0t}\frac{\partial^2u_{0c}}{\partial t^2}+\mathrm{I}_{1t}\frac{\partial^2u_{1c}}{\partial t^2}+\mathrm{I}_{2t}\frac{\partial^2u_{1t}}{\partial t^2}+\mathrm{I}_{0b}\frac{\partial^2u_{0c}}{\partial t^2}-\mathrm{I}_{1b}\frac{\partial^2u_{1c}}{\partial t^2}+\mathrm{I}_{2b}\frac{\partial^2u_{1b}}{\partial t^2}+\mathrm{I}_{0c}\frac{\partial^2u_{0c}}{\partial t^2}+$$

$$\mathrm{I}_{1c}\frac{\partial^2u_{1c}}{\partial t^2},$$

$$\delta v_{0c}:\frac{1}{r}\left(\frac{\partial}{\partial\theta}\left(\left(1+\tau_s\frac{\partial}{\partial t}\right)\left(\begin{array}{c}A_{12t}\dfrac{\partial u_{0c}}{\partial r}+B_{12t}\dfrac{\partial u_{1t}}{\partial r}+\dfrac{h_c}{2}A_{12t}\dfrac{\partial u_{1c}}{\partial r}+A_{22t}\dfrac{u_{0c}}{r}+B_{22t}\dfrac{u_{1t}}{r}\\+\dfrac{h_c}{2}A_{22t}\dfrac{u_{1c}}{r}+\dfrac{A_{22t}}{r}\dfrac{\partial v_{0c}}{\partial\theta}+\dfrac{B_{22t}}{r}\dfrac{\partial v_{1t}}{\partial\theta}+\dfrac{h_c}{2}\dfrac{A_{22t}}{r}\dfrac{\partial v_{1c}}{\partial\theta}\end{array}\right)\right)\right.$$

$$+\frac{1}{r}\left(\left(\left(1+\tau_s\frac{\partial}{\partial t}\right)\left(\frac{A_{66t}\left(\frac{\partial}{\partial\theta}u_{0c}\right)}{r}+\frac{B_{66t}\left(\frac{\partial}{\partial\theta}u_{1t}\right)}{r}+\frac{A_{66t}h_c\left(\frac{\partial}{\partial\theta}u_{1c}\right)}{2r}+A_{66t}\left(\frac{\partial}{\partial r}v_{0c}\right)\right.\right.\right.$$

$$\left.\left.\left.+B_{66t}\left(\frac{\partial}{\partial r}v_{1t}\right)+\frac{h_cA_{66t}\left(\frac{\partial}{\partial r}v_{1c}\right)}{2}-\frac{A_{66t}v_{0c}}{r}-\frac{B_{66t}v_{1t}}{r}-\frac{A_{66t}h_cv_{1c}}{2r}\right)\right) \quad (19d)$$

$$+r\left(\frac{\partial}{\partial r}\left(\left(1+\tau_s\frac{\partial}{\partial t}\right)\left(\frac{A_{66t}\left(\frac{\partial}{\partial\theta}u_{0c}\right)}{r}+\frac{B_{66t}\left(\frac{\partial}{\partial\theta}u_{1t}\right)}{r}+\frac{A_{66t}h_c\left(\frac{\partial}{\partial\theta}u_{1c}\right)}{2r}+A_{66t}\left(\frac{\partial}{\partial r}v_{0c}\right)\right.\right.\right.$$

$$\left.\left.\left.\left.+B_{66t}\left(\frac{\partial}{\partial r}v_{1t}\right)+\frac{h_cA_{66t}\left(\frac{\partial}{\partial r}v_{1c}\right)}{2}-\frac{A_{66t}v_{0c}}{r}-\frac{B_{66t}v_{1t}}{r}-\frac{A_{66t}h_cv_{1c}}{2r}\right)\right)\right)\right)$$

$$
\begin{aligned}
&+\frac{1}{r}\left(\left(1+\tau_s\frac{\partial}{\partial t}\right)\begin{pmatrix}\frac{A_{66t}\left(\frac{\partial}{\partial\theta}u_{0c}\right)}{r}+\frac{B_{66t}\left(\frac{\partial}{\partial\theta}u_{1t}\right)}{r}+\frac{A_{66t}h_c\left(\frac{\partial}{\partial\theta}u_{1c}\right)}{2r}+A_{66t}\left(\frac{\partial}{\partial r}v_{0c}\right)\\ +B_{66t}\left(\frac{\partial}{\partial r}v_{1t}\right)+\frac{h_cA_{66t}\left(\frac{\partial}{\partial r}v_{1c}\right)}{2}-\frac{A_{66t}v_{0c}}{r}-\frac{B_{66t}v_{1t}}{r}-\frac{A_{66t}h_cv_{1c}}{2r}\end{pmatrix}\right)\\
&\quad+\frac{1}{r}\left(\frac{\partial}{\partial\theta}\left(\left(1+\tau_s\frac{\partial}{\partial t}\right)\begin{pmatrix}A_{12c}\frac{\partial u_{0c}}{\partial r}+B_{12c}\frac{\partial u_{1c}}{\partial r}+A_{22c}\frac{u_{0c}}{r}\\ +B_{22c}\frac{u_{1c}}{r}+\frac{A_{22c}}{r}\frac{\partial v_{0c}}{\partial\theta}+\frac{B_{22c}}{r}\frac{\partial v_{1c}}{\partial\theta}\end{pmatrix}\right)\right)\\
&\quad+\frac{1}{r}\left(\left(\left(1+\tau_s\frac{\partial}{\partial t}\right)\begin{pmatrix}\frac{A_{66c}\left(\frac{\partial}{\partial\theta}u_{0c}\right)}{r}+\frac{B_{66c}\left(\frac{\partial}{\partial\theta}u_{1c}\right)}{r}+A_{66c}\left(\frac{\partial}{\partial r}v_{0c}\right)\\ +B_{66c}\left(\frac{\partial}{\partial r}v_{1t}\right)-\frac{A_{66c}v_{0c}}{r}-\frac{B_{66c}v_{1c}}{r}\end{pmatrix}\right)\right)\\
&\quad+r\left(\frac{\partial}{\partial r}\left(\left(1+\tau_s\frac{\partial}{\partial t}\right)\begin{pmatrix}\frac{A_{66c}\left(\frac{\partial}{\partial\theta}u_{0c}\right)}{r}+\frac{B_{66c}\left(\frac{\partial}{\partial\theta}u_{1c}\right)}{r}+A_{66c}\left(\frac{\partial}{\partial r}v_{0c}\right)\\ +B_{66c}\left(\frac{\partial}{\partial r}v_{1t}\right)-\frac{A_{66c}v_{0c}}{r}-\frac{B_{66c}v_{1c}}{r}\end{pmatrix}\right)\right)\right)\\
&\quad+\frac{1}{r}\left(\left(1+\tau_s\frac{\partial}{\partial t}\right)\begin{pmatrix}\frac{A_{66c}\left(\frac{\partial}{\partial\theta}u_{0c}\right)}{r}+\frac{B_{66c}\left(\frac{\partial}{\partial\theta}u_{1c}\right)}{r}+A_{66c}\left(\frac{\partial}{\partial r}v_{0c}\right)\\ +B_{66c}\left(\frac{\partial}{\partial r}v_{1t}\right)-\frac{A_{66c}v_{0c}}{r}-\frac{B_{66c}v_{1c}}{r}\end{pmatrix}\right)\\
&\quad+\frac{1}{r}\left(\frac{\partial}{\partial\theta}\left(\left(1+\tau_s\frac{\partial}{\partial t}\right)\begin{pmatrix}A_{12b}\frac{\partial u_{0c}}{\partial r}+B_{12b}\frac{\partial u_{1b}}{\partial r}-\frac{h_c}{2}A_{12b}\frac{\partial u_{1c}}{\partial r}\\ +A_{22b}\frac{u_{0c}}{r}+B_{22b}\frac{u_{1t}}{r}-\frac{h_c}{2}A_{22b}\frac{u_{1c}}{r}\\ +\frac{A_{22b}}{r}\frac{\partial v_{0c}}{\partial\theta}+\frac{B_{22b}}{r}\frac{\partial v_{1b}}{\partial\theta}-\frac{h_c}{2}\frac{A_{22b}}{r}\frac{\partial v_{1c}}{\partial\theta}\end{pmatrix}\right)\right)\\
&\quad+\frac{1}{r}\left(\left(\left(1+\tau_s\frac{\partial}{\partial t}\right)\begin{pmatrix}\frac{A_{66b}\left(\frac{\partial}{\partial\theta}u_{0c}\right)}{r}+\frac{B_{66b}\left(\frac{\partial}{\partial\theta}u_{1b}\right)}{r}-\frac{A_{66b}h_c\left(\frac{\partial}{\partial\theta}u_{1c}\right)}{2r}\\ +A_{66b}\left(\frac{\partial}{\partial r}v_{0c}\right)+B_{66b}\left(\frac{\partial}{\partial r}v_{1t}\right)-\frac{h_cA_{66b}\left(\frac{\partial}{\partial r}v_{1c}\right)}{2}\\ -\frac{A_{66b}v_{0c}}{r}-\frac{B_{66b}v_{1t}}{r}+\frac{A_{66b}h_cv_{1c}}{2r}\end{pmatrix}\right)\right)\\
&\quad+r\left(\frac{\partial}{\partial r}\left(\left(1+\tau_s\frac{\partial}{\partial t}\right)\begin{pmatrix}\frac{A_{66b}\left(\frac{\partial}{\partial\theta}u_{0c}\right)}{r}+\frac{B_{66b}\left(\frac{\partial}{\partial\theta}u_{1b}\right)}{r}-\frac{A_{66b}h_c\left(\frac{\partial}{\partial\theta}u_{1c}\right)}{2r}\\ +A_{66b}\left(\frac{\partial}{\partial r}v_{0c}\right)+B_{66b}\left(\frac{\partial}{\partial r}v_{1t}\right)-\frac{h_cA_{66b}\left(\frac{\partial}{\partial r}v_{1c}\right)}{2}\\ -\frac{A_{66b}v_{0c}}{r}-\frac{B_{66b}v_{1t}}{r}+\frac{A_{66b}h_cv_{1c}}{2r}\end{pmatrix}\right)\right)\right)\\
&+\frac{1}{r}\left(\left(1+\tau_s\frac{\partial}{\partial t}\right)\begin{pmatrix}\frac{A_{66b}\left(\frac{\partial}{\partial\theta}u_{0c}\right)}{r}+\frac{B_{66b}\left(\frac{\partial}{\partial\theta}u_{1b}\right)}{r}-\frac{A_{66b}h_c\left(\frac{\partial}{\partial\theta}u_{1c}\right)}{2r}+A_{66b}\left(\frac{\partial}{\partial r}v_{0c}\right)\\ +B_{66b}\left(\frac{\partial}{\partial r}v_{1t}\right)-\frac{h_cA_{66b}\left(\frac{\partial}{\partial r}v_{1c}\right)}{2}-\frac{A_{66b}v_{0c}}{r}-\frac{B_{66b}v_{1t}}{r}+\frac{A_{66b}h_cv_{1c}}{2r}\end{pmatrix}\right)
\end{aligned}
\tag{19d}
$$

$$= \mathrm{I}_{0t}\frac{\partial^2 v_{0c}}{\partial t^2} + \mathrm{I}_{1t}\frac{\partial^2 v_{1c}}{\partial t^2} + \mathrm{I}_{2t}\frac{\partial^2 v_{1t}}{\partial t^2} + \mathrm{I}_{0b}\frac{\partial^2 v_{0c}}{\partial t^2} - \mathrm{I}_{1b}\frac{\partial^2 v_{1c}}{\partial t^2} + \mathrm{I}_{2b}\frac{\partial^2 v_{1b}}{\partial t^2} + \mathrm{I}_{0c}\frac{\partial^2 v_{0c}}{\partial t^2} + \mathrm{I}_{1c}\frac{\partial^2 v_{1c}}{\partial t^2} \tag{19d}$$

$$\begin{aligned}\delta w_{0c}: &\frac{1}{r}\left(\left(\left(1+\tau_s\frac{\partial}{\partial t}\right)\left(A_{55t}u_{1t}+A_{55t}\frac{\partial w_{0c}}{\partial r}\right)\right)+r\left(\frac{\partial}{\partial r}\left(\left(1+\tau_s\frac{\partial}{\partial t}\right)\left(A_{55t}u_{1t}+A_{55t}\frac{\partial w_{0c}}{\partial r}\right)\right)\right)\right)+\\ &\frac{1}{r}\left(\frac{\partial}{\partial\theta}\left(\left(1+\tau_s\frac{\partial}{\partial t}\right)\left(A_{44t}v_{1t}+\frac{A_{44t}}{r}\frac{\partial w_{0c}}{\partial\theta}\right)\right)\right)+\frac{1}{r}\left(\left(\left(1+\tau_s\frac{\partial}{\partial t}\right)\left(A_{55c}u_{1c}+A_{55c}\frac{\partial w_{0c}}{\partial r}\right)\right)+r\left(\frac{\partial}{\partial r}\left(\left(1+\right.\right.\right.\right.\\ &\left.\left.\left.\left.\tau_s\frac{\partial}{\partial t}\right)\left(A_{55c}u_{1c}+A_{55c}\frac{\partial w_{0c}}{\partial r}\right)\right)\right)\right)+\frac{1}{r}\left(\frac{\partial}{\partial\theta}\left(\left(1+\tau_s\frac{\partial}{\partial t}\right)\left(A_{44t}v_{1c}+\frac{A_{44c}}{r}\frac{\partial w_{0c}}{\partial\theta}\right)\right)\right)+\frac{1}{r}\left(\left(\left(1+\right.\right.\right.\\ &\left.\left.\left.\tau_s\frac{\partial}{\partial t}\right)\left(A_{55b}u_{1b}+A_{55b}\frac{\partial w_{0c}}{\partial r}\right)\right)+r\left(\frac{\partial}{\partial r}\left(\left(1+\tau_s\frac{\partial}{\partial t}\right)\left(A_{55b}u_{1b}+A_{55b}\frac{\partial w_{0c}}{\partial r}\right)\right)\right)\right)+\frac{1}{r}\left(\frac{\partial}{\partial\theta}\left(\left(1+\right.\right.\right.\\ &\left.\left.\left.\tau_s\frac{\partial}{\partial t}\right)\left(A_{44t}v_{1b}+\frac{A_{44b}}{r}\frac{\partial w_{0c}}{\partial\theta}\right)\right)\right)-\mathrm{P}\left(\frac{1}{r}\frac{\partial w_{0c}}{\partial r}+\frac{\partial^2 w_{0c}}{\partial r^2}+\frac{1}{r^2}\frac{\partial^2 w_{0c}}{\partial\theta^2}\right)=\mathrm{I}_{0t}\frac{\partial^2 w_{0c}}{\partial t^2}+\mathrm{I}_{0c}\frac{\partial^2 w_{0c}}{\partial t^2}+\mathrm{I}_{0t}\frac{\partial^2 w_{0c}}{\partial t^2},\end{aligned} \tag{19e}$$

$$\begin{aligned}\delta u_{1c}: &\frac{h_c}{2r}\left(\left(\left(1+\tau_s\frac{\partial}{\partial t}\right)\begin{pmatrix}A_{11t}\frac{\partial u_{0c}}{\partial r}+B_{11t}\frac{\partial u_{1t}}{\partial r}+\frac{h_c}{2}A_{11t}\frac{\partial u_{1c}}{\partial r}+A_{12t}\frac{u_{0c}}{r}+B_{12t}\frac{u_{1t}}{r}\\ +\frac{h_c}{2}A_{12t}\frac{u_{1c}}{r}+\frac{A_{12t}}{r}\frac{\partial v_{0c}}{\partial\theta}+\frac{B_{12t}}{r}\frac{\partial v_{1t}}{\partial\theta}+\frac{h_c}{2}\frac{A_{12t}}{r}\frac{\partial v_{1c}}{\partial\theta}\end{pmatrix}\right)\right.\\ &+r\left(\frac{\partial}{\partial r}\left(\left(1+\tau_s\frac{\partial}{\partial t}\right)\begin{pmatrix}A_{11t}\frac{\partial u_{0c}}{\partial r}+B_{11t}\frac{\partial u_{1t}}{\partial r}+\frac{h_c}{2}A_{11t}\frac{\partial u_{1c}}{\partial r}\\ +A_{12t}\frac{u_{0c}}{r}+B_{12t}\frac{u_{1t}}{r}+\frac{h_c}{2}A_{12t}\frac{u_{1c}}{r}\\ +\frac{A_{12t}}{r}\frac{\partial v_{0c}}{\partial\theta}+\frac{B_{12t}}{r}\frac{\partial v_{1t}}{\partial\theta}+\frac{h_c}{2}\frac{A_{12t}}{r}\frac{\partial v_{1c}}{\partial\theta}\end{pmatrix}\right)\right)\\ &-\frac{h_c}{2r}\left(\left(1+\tau_s\frac{\partial}{\partial t}\right)\begin{pmatrix}A_{12t}\frac{\partial u_{0c}}{\partial r}+B_{12t}\frac{\partial u_{1t}}{\partial r}+\frac{h_c}{2}A_{12t}\frac{\partial u_{1c}}{\partial r}+A_{22t}\frac{u_{0c}}{r}+B_{22t}\frac{u_{1t}}{r}\\ +\frac{h_c}{2}A_{22t}\frac{u_{1c}}{r}+\frac{A_{22t}}{r}\frac{\partial v_{0c}}{\partial\theta}+\frac{B_{22t}}{r}\frac{\partial v_{1t}}{\partial\theta}+\frac{h_c}{2}\frac{A_{22t}}{r}\frac{\partial v_{1c}}{\partial\theta}\end{pmatrix}\right)\\ &+\frac{h_c}{2r}\left(\frac{\partial}{\partial\theta}\left(\left(1+\tau_s\frac{\partial}{\partial t}\right)\begin{pmatrix}\frac{A_{66t}\left(\frac{\partial}{\partial\theta}u_{0c}\right)}{r}+\frac{B_{66t}\left(\frac{\partial}{\partial\theta}u_{1t}\right)}{r}+\frac{A_{66t}h_c\left(\frac{\partial}{\partial\theta}u_{1c}\right)}{2r}\\ +A_{66t}\left(\frac{\partial}{\partial r}v_{0c}\right)+B_{66t}\left(\frac{\partial}{\partial r}v_{1t}\right)+\frac{h_cA_{66t}\left(\frac{\partial}{\partial r}v_{1c}\right)}{2}\\ -\frac{A_{66t}v_{0c}}{r}-\frac{B_{66t}v_{1t}}{r}-\frac{A_{66t}h_cv_{1c}}{2r}\end{pmatrix}\right)\right)\\ &+\frac{1}{r}\left(\left(\left(1+\tau_s\frac{\partial}{\partial t}\right)\begin{pmatrix}B_{11c}\frac{\partial u_{0c}}{\partial r}+C_{11c}\frac{\partial u_{1c}}{\partial r}+B_{12c}\frac{u_{0c}}{r}\\ +C_{12c}\frac{u_{1c}}{r}+\frac{B_{12c}}{r}\frac{\partial v_{0c}}{\partial\theta}+\frac{C_{12c}}{r}\frac{\partial v_{1c}}{\partial\theta}\end{pmatrix}\right)\right.\\ &\left.\left.+r\left(\frac{\partial}{\partial r}\left(\left(1+\tau_s\frac{\partial}{\partial t}\right)\begin{pmatrix}B_{11c}\frac{\partial u_{0c}}{\partial r}+C_{11c}\frac{\partial u_{1c}}{\partial r}+B_{12c}\frac{u_{0c}}{r}\\ +C_{12c}\frac{u_{1c}}{r}+\frac{B_{12c}}{r}\frac{\partial v_{0c}}{\partial\theta}+\frac{C_{12c}}{r}\frac{\partial v_{1c}}{\partial\theta}\end{pmatrix}\right)\right)\right)\right)\end{aligned} \tag{19f}$$

$$-\frac{1}{r}\left(\left(1+\tau_s\frac{\partial}{\partial t}\right)\begin{pmatrix}B_{12c}\frac{\partial u_{0c}}{\partial r}+C_{12c}\frac{\partial u_{1c}}{\partial r}+B_{22c}\frac{u_{0c}}{r}\\+C_{22c}\frac{u_{1c}}{r}+\frac{B_{22c}}{r}\frac{\partial v_{0c}}{\partial\theta}+\frac{C_{22c}}{r}\frac{\partial v_{1c}}{\partial\theta}\end{pmatrix}\right)+\frac{1}{r}\left(\frac{\partial}{\partial\theta}\left(\left(1+\tau_s\frac{\partial}{\partial t}\right)\left(\frac{B_{66c}\left(\frac{\partial}{\partial\theta}u_{0c}\right)}{r}+\frac{C_{66c}\left(\frac{\partial}{\partial\theta}u_{1c}\right)}{r}+\right.\right.\right.$$
$$\left.\left.\left.B_{66c}\left(\frac{\partial}{\partial r}v_{0c}\right)+C_{66c}\left(\frac{\partial}{\partial r}v_{1t}\right)-\frac{B_{66c}v_{0c}}{r}-\frac{C_{66c}v_{1c}}{r}\right)\right)\right)-\left(\left(1+\tau_s\frac{\partial}{\partial t}\right)\left(A_{55c}u_{1c}+A_{55c}\frac{\partial w_{0c}}{\partial r}\right)\right)-$$
$$\frac{h_c}{2r}\left(\left(\left(1+\tau_s\frac{\partial}{\partial t}\right)\left(A_{11b}\frac{\partial u_{0c}}{\partial r}+B_{11b}\frac{\partial u_{1b}}{\partial r}-\frac{h_c}{2}A_{11b}\frac{\partial u_{1c}}{\partial r}+A_{12b}\frac{u_{0c}}{r}+B_{12b}\frac{u_{1t}}{r}-\frac{h_c}{2}A_{12b}\frac{u_{1c}}{r}+\frac{A_{12b}}{r}\frac{\partial v_{0c}}{\partial\theta}+\right.\right.\right.$$
$$\left.\left.\left.\frac{B_{12b}}{r}\frac{\partial v_{1b}}{\partial\theta}-\frac{h_c}{2}\frac{A_{12b}}{r}\frac{\partial v_{1c}}{\partial\theta}\right)\right)+r\left(\frac{\partial}{\partial r}\left(\left(1+\tau_s\frac{\partial}{\partial t}\right)\left(A_{11b}\frac{\partial u_{0c}}{\partial r}+B_{11b}\frac{\partial u_{1b}}{\partial r}-\frac{h_c}{2}A_{11b}\frac{\partial u_{1c}}{\partial r}+A_{12b}\frac{u_{0c}}{r}+\right.\right.\right.\right.$$
$$\left.\left.\left.\left.B_{12b}\frac{u_{1t}}{r}-\frac{h_c}{2}A_{12b}\frac{u_{1c}}{r}+\frac{A_{12b}}{r}\frac{\partial v_{0c}}{\partial\theta}+\frac{B_{12b}}{r}\frac{\partial v_{1b}}{\partial\theta}-\frac{h_c}{2}\frac{A_{12b}}{r}\frac{\partial v_{1c}}{\partial\theta}\right)\right)\right)\right)+\frac{h_c}{2r}\left(\left(1+\tau_s\frac{\partial}{\partial t}\right)\left(A_{12b}\frac{\partial u_{0c}}{\partial r}+\right.\right.$$
$$\left.\left.B_{12b}\frac{\partial u_{1b}}{\partial r}-\frac{h_c}{2}A_{12b}\frac{\partial u_{1c}}{\partial r}+A_{22b}\frac{u_{0c}}{r}+B_{22b}\frac{u_{1t}}{r}-\frac{h_c}{2}A_{22b}\frac{u_{1c}}{r}+\frac{A_{22b}}{r}\frac{\partial v_{0c}}{\partial\theta}+\frac{B_{22b}}{r}\frac{\partial v_{1b}}{\partial\theta}-\frac{h_c}{2}\frac{A_{22b}}{r}\frac{\partial v_{1c}}{\partial\theta}\right)\right)-$$
$$\frac{h_c}{2r}\left(\frac{\partial}{\partial\theta}\left(\left(1+\tau_s\frac{\partial}{\partial t}\right)\left(\frac{A_{66b}\left(\frac{\partial}{\partial\theta}u_{0c}\right)}{r}+\frac{B_{66b}\left(\frac{\partial}{\partial\theta}u_{1b}\right)}{r}-\frac{A_{66b}h_c\left(\frac{\partial}{\partial\theta}u_{1c}\right)}{2r}+A_{66b}\left(\frac{\partial}{\partial r}v_{0c}\right)+B_{66b}\left(\frac{\partial}{\partial r}v_{1t}\right)-\right.\right.\right.$$
$$\left.\left.\left.\left.\frac{h_cA_{66b}\left(\frac{\partial}{\partial r}v_{1c}\right)}{2}-\frac{A_{66b}v_{0c}}{r}-\frac{B_{66b}v_{1t}}{r}+\frac{A_{66b}h_cv_{1c}}{2r}\right)\right)\right)=\mathrm{J}_{0t}\frac{\partial^2u_{0c}}{\partial t^2}+\mathrm{J}_{1t}\frac{\partial^2u_{1c}}{\partial t^2}+\mathrm{J}_{2t}\frac{\partial^2u_{1t}}{\partial t^2}-\mathrm{J}_{0b}\frac{\partial^2u_{0c}}{\partial t^2}+$$
$$\mathrm{J}_{1b}\frac{\partial^2u_{1c}}{\partial t^2}-\mathrm{J}_{2b}\frac{\partial^2u_{1b}}{\partial t^2}+\mathrm{I}_{1c}\frac{\partial^2u_{0c}}{\partial t^2}+\mathrm{I}_{2c}\frac{\partial^2u_{1c}}{\partial t^2}, \tag{19f}$$

$$\delta v_{1c}:\frac{h_c}{2r}\left(\frac{\partial}{\partial\theta}\left(\left(1+\tau_s\frac{\partial}{\partial t}\right)\begin{pmatrix}A_{12t}\frac{\partial u_{0c}}{\partial r}+B_{12t}\frac{\partial u_{1t}}{\partial r}+\frac{h_c}{2}A_{12t}\frac{\partial u_{1c}}{\partial r}+A_{22t}\frac{u_{0c}}{r}+B_{22t}\frac{u_{1t}}{r}\\+\frac{h_c}{2}A_{22t}\frac{u_{1c}}{r}+\frac{A_{22t}}{r}\frac{\partial v_{0c}}{\partial\theta}+\frac{B_{22t}}{r}\frac{\partial v_{1t}}{\partial\theta}+\frac{h_c}{2}\frac{A_{22t}}{r}\frac{\partial v_{1c}}{\partial\theta}\end{pmatrix}\right)\right)$$
$$+\frac{h_c}{2r}\left(\left(\left(1+\tau_s\frac{\partial}{\partial t}\right)\begin{pmatrix}\frac{A_{66t}\left(\frac{\partial}{\partial\theta}u_{0c}\right)}{r}+\frac{B_{66t}\left(\frac{\partial}{\partial\theta}u_{1t}\right)}{r}+\frac{A_{66t}h_c\left(\frac{\partial}{\partial\theta}u_{1c}\right)}{2r}\\+A_{66t}\left(\frac{\partial}{\partial r}v_{0c}\right)+B_{66t}\left(\frac{\partial}{\partial r}v_{1t}\right)+\frac{h_cA_{66t}\left(\frac{\partial}{\partial r}v_{1c}\right)}{2}\\-\frac{A_{66t}v_{0c}}{r}-\frac{B_{66t}v_{1t}}{r}-\frac{A_{66t}h_cv_{1c}}{2r}\end{pmatrix}\right)\right)$$
$$+r\left(\frac{\partial}{\partial r}\left(\left(1+\tau_s\frac{\partial}{\partial t}\right)\begin{pmatrix}\frac{A_{66t}\left(\frac{\partial}{\partial\theta}u_{0c}\right)}{r}+\frac{B_{66t}\left(\frac{\partial}{\partial\theta}u_{1t}\right)}{r}+\frac{A_{66t}h_c\left(\frac{\partial}{\partial\theta}u_{1c}\right)}{2r}\\+A_{66t}\left(\frac{\partial}{\partial r}v_{0c}\right)+B_{66t}\left(\frac{\partial}{\partial r}v_{1t}\right)+\frac{h_cA_{66t}\left(\frac{\partial}{\partial r}v_{1c}\right)}{2}\\-\frac{A_{66t}v_{0c}}{r}-\frac{B_{66t}v_{1t}}{r}-\frac{A_{66t}h_cv_{1c}}{2r}\end{pmatrix}\right)\right)\right)$$
$$+\frac{h_c}{2r}\left(\left(1+\tau_s\frac{\partial}{\partial t}\right)\left(\frac{A_{66t}\left(\frac{\partial}{\partial\theta}u_{0c}\right)}{r}+\frac{B_{66t}\left(\frac{\partial}{\partial\theta}u_{1t}\right)}{r}+\frac{A_{66t}h_c\left(\frac{\partial}{\partial\theta}u_{1c}\right)}{2r}+A_{66t}\left(\frac{\partial}{\partial r}v_{0c}\right)\right.\right.$$
$$\left.\left.+B_{66t}\left(\frac{\partial}{\partial r}v_{1t}\right)+\frac{h_cA_{66t}\left(\frac{\partial}{\partial r}v_{1c}\right)}{2}-\frac{A_{66t}v_{0c}}{r}-\frac{B_{66t}v_{1t}}{r}-\frac{A_{66t}h_cv_{1c}}{2r}\right)\right) \tag{19g}$$

$$+\frac{1}{r}\left(\frac{\partial}{\partial\theta}\left(\left(1+\tau_s\frac{\partial}{\partial t}\right)\left(B_{12c}\frac{\partial u_{0c}}{\partial r}+C_{12c}\frac{\partial u_{1c}}{\partial r}+B_{22c}\frac{u_{0c}}{r}+C_{22c}\frac{u_{1c}}{r}+\frac{B_{22c}}{r}\frac{\partial v_{0c}}{\partial\theta}+\frac{C_{22c}}{r}\frac{\partial v_{1c}}{\partial\theta}\right)\right)\right)+\frac{1}{r}\left(\left(\left(1+\right.\right.\right.$$
$$\left.\left.\left.\tau_s\frac{\partial}{\partial t}\right)\left(\frac{B_{66c}\left(\frac{\partial}{\partial\theta}u_{0c}\right)}{r}+\frac{C_{66c}\left(\frac{\partial}{\partial\theta}u_{1c}\right)}{r}+B_{66c}\left(\frac{\partial}{\partial r}v_{0c}\right)+C_{66c}\left(\frac{\partial}{\partial r}v_{1t}\right)-\frac{B_{66c}v_{0c}}{r}-\frac{C_{66c}v_{1c}}{r}\right)\right)+r\left(\frac{\partial}{\partial r}\left(\left(1+\right.\right.\right.\right.$$
$$\left.\left.\left.\left.\tau_s\frac{\partial}{\partial t}\right)\left(\frac{B_{66c}\left(\frac{\partial}{\partial\theta}u_{0c}\right)}{r}+\frac{C_{66c}\left(\frac{\partial}{\partial\theta}u_{1c}\right)}{r}+B_{66c}\left(\frac{\partial}{\partial r}v_{0c}\right)+C_{66c}\left(\frac{\partial}{\partial r}v_{1t}\right)-\frac{B_{66c}v_{0c}}{r}-\frac{C_{66c}v_{1c}}{r}\right)\right)\right)\right)+\frac{1}{r}\left(\left(1+\right.\right.$$
$$\left.\left.\tau_s\frac{\partial}{\partial t}\right)\left(\frac{B_{66c}\left(\frac{\partial}{\partial\theta}u_{0c}\right)}{r}+\frac{C_{66c}\left(\frac{\partial}{\partial\theta}u_{1c}\right)}{r}+B_{66c}\left(\frac{\partial}{\partial r}v_{0c}\right)+C_{66c}\left(\frac{\partial}{\partial r}v_{1t}\right)-\frac{B_{66c}v_{0c}}{r}-\frac{C_{66c}v_{1c}}{r}\right)\right)-\left(\left(1+\right.\right.$$
$$\left.\left.\tau_s\frac{\partial}{\partial t}\right)\left(A_{44t}v_{1c}+\frac{A_{44c}}{r}\frac{\partial w_{0c}}{\partial\theta}\right)\right)-\frac{1}{2r}h_c\left(\frac{\partial}{\partial\theta}\left(\left(1+\tau_s\frac{\partial}{\partial t}\right)\left(A_{12b}\frac{\partial u_{0c}}{\partial r}+B_{12b}\frac{\partial u_{1b}}{\partial r}-\frac{h_c}{2}A_{12b}\frac{\partial u_{1c}}{\partial r}+A_{22b}\frac{u_{0c}}{r}+\right.\right.\right.$$
$$\left.\left.\left.B_{22b}\frac{u_{1t}}{r}-\frac{h_c}{2}A_{22b}\frac{u_{1c}}{r}+\frac{A_{22b}}{r}\frac{\partial v_{0c}}{\partial\theta}+\frac{B_{22b}}{r}\frac{\partial v_{1b}}{\partial\theta}-\frac{h_c}{2}\frac{A_{22b}}{r}\frac{\partial v_{1c}}{\partial\theta}\right)\right)-\frac{h_c}{2r}\left(\left(\left(1+\tau_s\frac{\partial}{\partial t}\right)\left(\frac{A_{66b}\left(\frac{\partial}{\partial\theta}u_{0c}\right)}{r}+\right.\right.\right.\right. \tag{19g}$$
$$\left.\left.\left.\left.\frac{B_{66b}\left(\frac{\partial}{\partial\theta}u_{1b}\right)}{r}-\frac{A_{66b}h_c\left(\frac{\partial}{\partial\theta}u_{1c}\right)}{2r}+A_{66b}\left(\frac{\partial}{\partial r}v_{0c}\right)+B_{66b}\left(\frac{\partial}{\partial r}v_{1t}\right)-\frac{h_cA_{66b}\left(\frac{\partial}{\partial r}v_{1c}\right)}{2}-\frac{A_{66b}v_{0c}}{r}-\frac{B_{66b}v_{1t}}{r}+\right.\right.\right.$$
$$\left.\left.\left.\left.\frac{A_{66b}h_cv_{1c}}{2r}\right)\right)+r\left(\frac{\partial}{\partial r}\left(\left(1+\tau_s\frac{\partial}{\partial t}\right)\left(\frac{A_{66b}\left(\frac{\partial}{\partial\theta}u_{0c}\right)}{r}+\frac{B_{66b}\left(\frac{\partial}{\partial\theta}u_{1b}\right)}{r}-\frac{A_{66b}h_c\left(\frac{\partial}{\partial\theta}u_{1c}\right)}{2r}+A_{66b}\left(\frac{\partial}{\partial r}v_{0c}\right)+\right.\right.\right.\right.$$
$$\left.\left.\left.\left.\left.B_{66b}\left(\frac{\partial}{\partial r}v_{1t}\right)-\frac{h_cA_{66b}\left(\frac{\partial}{\partial r}v_{1c}\right)}{2}-\frac{A_{66b}v_{0c}}{r}-\frac{B_{66b}v_{1t}}{r}+\frac{A_{66b}h_cv_{1c}}{2r}\right)\right)\right)\right)-\frac{h_c}{2r}\left(\left(1+\tau_s\frac{\partial}{\partial t}\right)\left(\frac{A_{66b}\left(\frac{\partial}{\partial\theta}u_{0c}\right)}{r}+\right.\right.$$
$$\left.\left.\frac{B_{66b}\left(\frac{\partial}{\partial\theta}u_{1b}\right)}{r}-\frac{A_{66b}h_c\left(\frac{\partial}{\partial\theta}u_{1c}\right)}{2r}+A_{66b}\left(\frac{\partial}{\partial r}v_{0c}\right)+B_{66b}\left(\frac{\partial}{\partial r}v_{1t}\right)-\frac{h_cA_{66b}\left(\frac{\partial}{\partial r}v_{1c}\right)}{2}-\frac{A_{66b}v_{0c}}{r}-\frac{B_{66b}v_{1t}}{r}+\right.$$
$$\left.\left.\frac{A_{66b}h_cv_{1c}}{2r}\right)\right)=\mathrm{J}_{0t}\frac{\partial^2v_{0c}}{\partial t^2}+\mathrm{J}_{1t}\frac{\partial^2v_{1c}}{\partial t^2}+\mathrm{J}_{2t}\frac{\partial^2v_{1t}}{\partial t^2}-\mathrm{J}_{0b}\frac{\partial^2v_{0c}}{\partial t^2}+\mathrm{J}_{1b}\frac{\partial^2v_{1c}}{\partial t^2}-\mathrm{J}_{2b}\frac{\partial^2v_{1b}}{\partial t^2}+\mathrm{I}_{1c}\frac{\partial^2v_{0c}}{\partial t^2}+\mathrm{I}_{2c}\frac{\partial^2v_{1c}}{\partial t^2},$$

$$\delta u_{1b}:\frac{1}{r}\left(\left(\left(1+\tau_s\frac{\partial}{\partial t}\right)\left(\begin{array}{c}B_{11b}\dfrac{\partial u_{0c}}{\partial r}+C_{11b}\dfrac{\partial u_{1b}}{\partial r}-\dfrac{h_c}{2}B_{11b}\dfrac{\partial u_{1c}}{\partial r}+B_{12b}\dfrac{u_{0c}}{r}+C_{12b}\dfrac{u_{1t}}{r}\\ -\dfrac{h_c}{2}B_{12b}\dfrac{u_{1c}}{r}+\dfrac{B_{12b}}{r}\dfrac{\partial v_{0c}}{\partial\theta}+\dfrac{C_{12b}}{r}\dfrac{\partial v_{1b}}{\partial\theta}-\dfrac{h_c}{2}\dfrac{B_{12b}}{r}\dfrac{\partial v_{1c}}{\partial\theta}\end{array}\right)\right)\right.$$
$$\left.+r\left(\frac{\partial}{\partial r}\left(\left(1+\tau_s\frac{\partial}{\partial t}\right)\left(\begin{array}{c}B_{11b}\dfrac{\partial u_{0c}}{\partial r}+C_{11b}\dfrac{\partial u_{1b}}{\partial r}-\dfrac{h_c}{2}B_{11b}\dfrac{\partial u_{1c}}{\partial r}\\ +B_{12b}\dfrac{u_{0c}}{r}+C_{12b}\dfrac{u_{1t}}{r}-\dfrac{h_c}{2}B_{12b}\dfrac{u_{1c}}{r}\\ +\dfrac{B_{12b}}{r}\dfrac{\partial v_{0c}}{\partial\theta}+\dfrac{C_{12b}}{r}\dfrac{\partial v_{1b}}{\partial\theta}-\dfrac{h_c}{2}\dfrac{B_{12b}}{r}\dfrac{\partial v_{1c}}{\partial\theta}\end{array}\right)\right)\right)\right) \tag{19h}$$
$$-\frac{1}{r}\left(\left(1+\tau_s\frac{\partial}{\partial t}\right)\left(B_{12b}\frac{\partial u_{0c}}{\partial r}+C_{12b}\frac{\partial u_{1b}}{\partial r}-\frac{h_c}{2}B_{12b}\frac{\partial u_{1c}}{\partial r}+B_{22b}\frac{u_{0c}}{r}+C_{22b}\frac{u_{1t}}{r}\right.\right.$$
$$\left.\left.-\frac{h_c}{2}B_{22b}\frac{u_{1c}}{r}+\frac{B_{22b}}{r}\frac{\partial v_{0c}}{\partial\theta}+\frac{C_{22b}}{r}\frac{\partial v_{1b}}{\partial\theta}-\frac{h_c}{2}\frac{B_{22b}}{r}\frac{\partial v_{1c}}{\partial\theta}\right)\right)$$

$$+\frac{1}{r}\left(\frac{\partial}{\partial\theta}\left(\left(1+\tau_s\frac{\partial}{\partial t}\right)\begin{pmatrix}\frac{B_{66b}\left(\frac{\partial}{\partial\theta}u_{0c}\right)}{r}+\frac{C_{66b}\left(\frac{\partial}{\partial\theta}u_{1b}\right)}{r}-\frac{B_{66b}h_c\left(\frac{\partial}{\partial\theta}u_{1c}\right)}{2r}+B_{66b}\left(\frac{\partial}{\partial r}v_{0c}\right)\\+C_{66b}\left(\frac{\partial}{\partial r}v_{1t}\right)-\frac{h_cB_{66b}\left(\frac{\partial}{\partial r}v_{1c}\right)}{2}-\frac{B_{66b}v_{0c}}{r}-\frac{C_{66b}v_{1t}}{r}+\frac{B_{66b}h_cv_{1c}}{2r}\end{pmatrix}\right)\right)-\left(\left(1+\right.\right.$$
$$\left.\left.\tau_s\frac{\partial}{\partial t}\right)\left(A_{55b}u_{1b}+A_{55b}\frac{\partial w_{0c}}{\partial r}\right)\right)=\mathrm{K}_{0b}\frac{\partial^2u_{0c}}{\partial t^2}-\mathrm{K}_{1b}\frac{\partial^2u_{1c}}{\partial t^2}+\mathrm{K}_{2b}\frac{\partial^2u_{1b}}{\partial t^2}, \tag{19h}$$

$$\delta v_{1b}:\frac{1}{r}\left(\frac{\partial}{\partial\theta}\left(\left(1+\tau_s\frac{\partial}{\partial t}\right)\left(B_{12b}\frac{\partial u_{0c}}{\partial r}+C_{12b}\frac{\partial u_{1b}}{\partial r}-\frac{h_c}{2}B_{12b}\frac{\partial u_{1c}}{\partial r}+B_{22b}\frac{u_{0c}}{r}+C_{22b}\frac{u_{1t}}{r}-\frac{h_c}{2}B_{22b}\frac{u_{1c}}{r}+\right.\right.\right.$$
$$\left.\left.\left.\frac{B_{22b}}{r}\frac{\partial v_{0c}}{\partial\theta}+\frac{C_{22b}}{r}\frac{\partial v_{1b}}{\partial\theta}-\frac{h_c}{2}\frac{B_{22b}}{r}\frac{\partial v_{1c}}{\partial\theta}\right)\right)\right)+\frac{1}{r}\left(\left(\left(1+\tau_s\frac{\partial}{\partial t}\right)\left(\frac{B_{66b}\left(\frac{\partial}{\partial\theta}u_{0c}\right)}{r}+\frac{C_{66b}\left(\frac{\partial}{\partial\theta}u_{1b}\right)}{r}-\frac{B_{66b}h_c\left(\frac{\partial}{\partial\theta}u_{1c}\right)}{2r}+\right.\right.\right.$$
$$\left.\left.\left.B_{66b}\left(\frac{\partial}{\partial r}v_{0c}\right)+C_{66b}\left(\frac{\partial}{\partial r}v_{1t}\right)-\frac{h_cB_{66b}\left(\frac{\partial}{\partial r}v_{1c}\right)}{2}-\frac{B_{66b}v_{0c}}{r}-\frac{C_{66b}v_{1t}}{r}+\frac{B_{66b}h_cv_{1c}}{2r}\right)\right)+r\left(\frac{\partial}{\partial r}\left(\left(1+\right.\right.\right.\right.$$
$$\left.\left.\left.\left.\tau_s\frac{\partial}{\partial t}\right)\left(\frac{B_{66b}\left(\frac{\partial}{\partial\theta}u_{0c}\right)}{r}+\frac{C_{66b}\left(\frac{\partial}{\partial\theta}u_{1b}\right)}{r}-\frac{B_{66b}h_c\left(\frac{\partial}{\partial\theta}u_{1c}\right)}{2r}+B_{66b}\left(\frac{\partial}{\partial r}v_{0c}\right)+C_{66b}\left(\frac{\partial}{\partial r}v_{1t}\right)-\frac{h_cB_{66b}\left(\frac{\partial}{\partial r}v_{1c}\right)}{2}-\frac{B_{66b}v_{0c}}{r}-\right.\right.\right.\right.\tag{19i}$$
$$\left.\left.\left.\left.\frac{C_{66b}v_{1t}}{r}+\frac{B_{66b}h_cv_{1c}}{2r}\right)\right)\right)\right)+\frac{1}{r}\left(\left(1+\tau_s\frac{\partial}{\partial t}\right)\left(\frac{B_{66b}\left(\frac{\partial}{\partial\theta}u_{0c}\right)}{r}+\frac{C_{66b}\left(\frac{\partial}{\partial\theta}u_{1b}\right)}{r}-\frac{B_{66b}h_c\left(\frac{\partial}{\partial\theta}u_{1c}\right)}{2r}+B_{66b}\left(\frac{\partial}{\partial r}v_{0c}\right)+\right.\right.$$
$$\left.\left.C_{66b}\left(\frac{\partial}{\partial r}v_{1t}\right)-\frac{h_cB_{66b}\left(\frac{\partial}{\partial r}v_{1c}\right)}{2}-\frac{B_{66b}v_{0c}}{r}-\frac{C_{66b}v_{1t}}{r}+\frac{B_{66b}h_cv_{1c}}{2r}\right)\right)-\left(\left(1+\tau_s\frac{\partial}{\partial t}\right)\left(A_{44t}v_{1b}+\frac{A_{44b}}{r}\frac{\partial w_{0c}}{\partial\theta}\right)\right)=$$
$$\mathrm{K}_{0b}\frac{\partial^2v_{0c}}{\partial t^2}-\mathrm{K}_{1b}\frac{\partial^2v_{1c}}{\partial t^2}+\mathrm{K}_{2b}\frac{\partial^2v_{1b}}{\partial t^2},$$

Also, general associated boundary conditions can be given by:

$$\delta u_{1t}:(rM_{rrt})n_r+\left(\frac{M_{r\theta t}}{r}\right)n_\theta=0, \tag{20a}$$

$$\delta v_{1t}:(M_{r\theta t})n_r+\left(\frac{M_{\theta\theta t}}{r}\right)n_\theta=0, \tag{20b}$$

$$\delta u_{0c}:(N_{rrt}+N_{rrc}+N_{rrb})n_r+\left(\frac{N_{r\theta t}}{r}+\frac{N_{r\theta c}}{r}+\frac{N_{r\theta b}}{r}\right)n_\theta=0, \tag{20c}$$

$$\delta v_{0c}:(N_{r\theta t}+N_{r\theta c}+N_{r\theta b})n_r+\left(\frac{N_{\theta\theta t}}{r}+\frac{N_{\theta\theta c}}{r}+\frac{N_{\theta\theta b}}{r}\right)n_\theta=0, \tag{20d}$$

$$\delta w_{0c}:(N_{rzt}+N_{rzc}+N_{rzb})n_r+\left(\frac{N_{\theta zt}}{r}+\frac{N_{\theta zc}}{r}+\frac{N_{\theta zb}}{r}\right)n_\theta=0, \tag{20e}$$

$$\delta u_{1c}:\left(\frac{h_c}{2}N_{rrt}+M_{rrc}-\frac{h_c}{2}N_{rrb}\right)n_r+\left(\frac{h_c}{2}\frac{N_{r\theta t}}{r}+\frac{M_{r\theta c}}{r}-\frac{h_c}{2}\frac{N_{r\theta b}}{r}\right)n_\theta=0, \tag{20f}$$

$$\delta v_{1c}:\left(\frac{h_c}{2}N_{r\theta t}+M_{r\theta c}-\frac{h_c}{2}N_{r\theta b}\right)n_r+\left(\frac{h_c}{2}\frac{N_{\theta\theta t}}{r}+\frac{M_{\theta\theta c}}{r}-\frac{h_c}{2}\frac{N_{\theta\theta b}}{r}\right)n_\theta=0, \tag{20g}$$

$$\delta u_{1t}:(rM_{rrb})n_r+\left(\frac{M_{r\theta b}}{r}\right)n_\theta=0, \tag{20h}$$

$$\delta v_{1t}:(M_{r\theta b})n_r+\left(\frac{M_{\theta\theta b}}{r}\right)n_\theta=0. \tag{20i}$$

3. Solution procedure

GDQ method as the strong solver can be used in Refs.

(Feng *et al*. 2021a, b, He *et al*. 2020, Weng *et al*. 2021). In the current section of this scrutinization, we demonstrated a solution technique known as GDQ model to solve the current problem's equations. GDQ method as the strong solver can be used for solving various systems and structures. In this technique have (Shu 2012):

$$\frac{\partial^n f}{\partial r^n} = \sum_{m=1}^{M} C^{(n)}{}_{j,m} f_{m,k} \tag{21}$$

In which, $C^{(n)}$ denotes weighting elements for the n^{th}-order derivative in the direction of radius, that would be derived as below:

$$\begin{aligned} C_{ij}^{(1)} &= -\sum_{i\neq j, j=1}^{n} C_{ij}^{(1)} \; j = i \\ C_{ij}^{(1)} &= \frac{M(x_i)}{(-x_j + x_i)M(x_j)} j, i = 1,2,\ldots,n \quad , j \neq i \end{aligned} \tag{22}$$

where,

$$M(x_i) = \prod_{j=1, j\neq i}^{n} (x_i - x_j) \tag{23}$$

The derivatives of Eq. (21) would be given as the next relations (Feng *et al*. 2021c, Han *et al*. 2021, Jiang *et al*. 2021, Li *et al*. 2020, 2019):

$$\begin{aligned} &C_{ii}^{(n)} = -\sum_{j=1, i\neq j}^{n} C_{ij}^{(n)} \leq n \leq N-1 \\ &\text{while} j, i = 1,2,\ldots,N \\ &C_{ij}^{(n)} = r\left[C_{ij}^{(n-1)} C_{ij}^{(1)} - \frac{C_{ij}^{(n-1)}}{(x_i - x_j)}\right] \\ &i \neq j, 2 \leq n \leq N-1 \;\; \text{while} j, i = 1,2,\ldots,N. \end{aligned} \tag{24}$$

Moreover, Employing Chebyshev polynomials greed points, the seed through r-axes would be distributed as (Shu and Richards 1992):

$$\begin{aligned} r_i &= \frac{R_0 - R_i}{2}\left(1 - cos\left(\frac{(i-1)}{(N_i - 1)}\pi\right)\right) + R_i i \\ &= 1,2,3,\ldots,N_i \end{aligned} \tag{25}$$

Moreover, disk's displacement fields could be provided by (Dai and Safarpour 2021, Ebrahimi and Safarpour 2018, Huang *et al*. 2021b, Jiao *et al*. 2021, Moradi *et al*. 2021, Wang *et al*. 2021, Xu *et al*.2021, Zhang *et al*. 2021b, Zhao *et al*. 2021):

$$\begin{Bmatrix} u_0 \\ v_0 \\ w_0 \\ u_1 \\ v_1 \end{Bmatrix} = \sum_{n=1}^{\infty} \begin{Bmatrix} u_{0n}(R) \times sin(n\theta) \\ v_{0n}(R) \times cos(n\theta) \\ w_{0n}(R) \times sin(n\theta) \\ u_{1n}(R) \times sin(n\theta) \\ v_{1n}(R) \times cos(n\theta) \end{Bmatrix} e^{i\omega t} \tag{26}$$

Ultimately, the GDQ form of the final equations would be altered to (Hou *et al*. 2021, Huang *et al*. 2021c, Liu *et al*. 2021b, Ma *et al*. 2017, Safarpour *et al*. 2017a, b, Yu *et al*. 2022):

$$\begin{aligned} \left\{\begin{bmatrix} [C_{dd}] & [C_{db}] \\ [C_{bd}] & [C_{bb}] \end{bmatrix} \omega_n + \begin{bmatrix} [M_{dd}] & [M_{db}] \\ [M_{bd}] & [M_{bb}] \end{bmatrix} \omega_n^2 \right. \\ \left. + \begin{bmatrix} [K_{dd}] & [K_{db}] \\ [K_{bd}] & [K_{bb}] \end{bmatrix}\right\} \begin{Bmatrix} \delta_d \\ \delta_b \end{Bmatrix} = 0 \end{aligned} \tag{27}$$

M, *K*, and *C*, respectively, are the damping, stiffness, and mass matrixes. Then, by solving the next equation, system's frequency and displacement fields may be extracted employing GDQ technique.

$$K^* + M^* \omega^2 + C^* \omega = 0 \tag{28}$$

4. Fourth-order Runge-Kutta approach

The final relations of the current system would be defined as next equation:

$$M\ddot{X} + C\dot{X} + KX = 0 \tag{29}$$

By applying X=X_1 have:

$$M\ddot{X}_1 + C\dot{X}_1 + KX_1 = 0 \tag{30}$$

Then Eq. (34) separate into two first-order relations:

$$\dot{X}_1 = X_2 \tag{31a}$$

$$\dot{X}_2 = -\frac{C}{M} X_2 - \frac{K}{M} X_1 \tag{31b}$$

here:

$$X_1 = \begin{Bmatrix} \delta_d \\ \delta_b \end{Bmatrix}, X_2 = \begin{Bmatrix} \dot{\delta}_d \\ \dot{\delta}_b \end{Bmatrix}, \tag{32a}$$

$$\begin{aligned} C = \begin{bmatrix} [C_{dd}] & [C_{db}] \\ [C_{bd}] & [C_{bb}] \end{bmatrix}, M = \begin{bmatrix} [M_{dd}] & [M_{db}] \\ [M_{bd}] & [M_{bb}] \end{bmatrix}, K \\ = \begin{bmatrix} [K_{dd}] & [K_{db}] \\ [K_{bd}] & [K_{bb}] \end{bmatrix} \end{aligned} \tag{32b}$$

here the primary conditions would be $X_1(0) = 1$ and $\dot{X}_2(0) = 0$.

The problem's frequencies would be achieved as solutions of Eq. (29). Moreover, the non-dimensional frequency, dimensionless deflection could be given as follows:

$$\begin{aligned} \bar{\omega}_n &= \omega_n R_o^2 \sqrt{\frac{\rho_m}{E_m}} \\ \bar{W} &= \frac{W}{W_{max}} \end{aligned} \tag{33}$$

5. Deep learning-based comparative study

Deep learning can be used for predicting behavior of the complex systems and structures (Liu *et al*. 2020a, Mi *et al*. 2021, Ni *et al*. 2020a, b). Recently, a broad range of scientists and researchers have been attracted by deep learning to employ it as an applicable tool in multifarious fields including segmentation, regression and classification duties. Then, the authors would be able to design a deep neural network (DNN) considering optimization factors achieved by ADADELTA (an abbreviation for adaptive

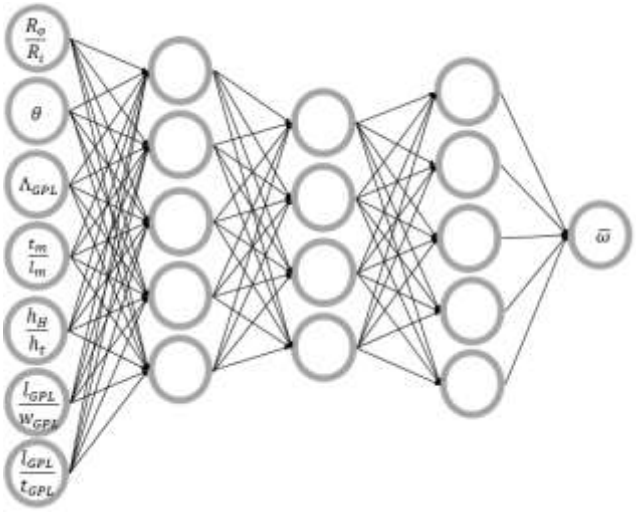

Fig. 2 The system configuration of the fully-connected deep neural network

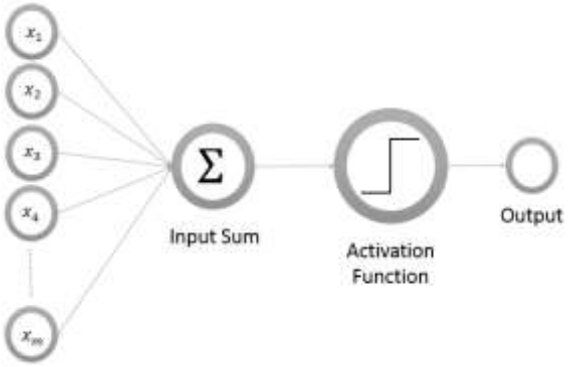

Fig. 3 Operation mechanism and elements of each perceptron (Wu 2021)

delta). Deep learning can be used for predicting the behavior of complex systems and structures (Shariati *et al*. 2012, 2016a, b, 2019, 2020g, 2021a, b). The set of $X = \left\{\frac{R_o}{R_i}, \theta, \Lambda_{GPL}, \frac{t_m}{l_m}, \frac{h_H}{h_t}, \frac{l_{GPL}}{w_{GPL}}, \frac{l_{GPL}}{t_{GPL}}\right\}^T$ could be selected as the regression-based DNN input to estimate the dimensionless frequency $\hat{Y} = \bar{\omega}$. The mentioned DNN schematic would be illustrated in Fig. 2.

All DNN layers have numerical units called perceptron. The next figure (Fig. 3) illustrates the details of operations conducted in each perceptron (Shariati *et al*. 2020d, e, f, h, i)

The perceptron input would be the output of the units constituting the last network layer. To achieve the computational output of the unit, the amount of each input should be mathematically operated with biases and weights. To obtain more knowledge regarding the basics of the neural network technique, readers can take a look the contents of (Wu 2021) as the reference. The mean squared error (MSE) would be the metric chosen in this research to examine the DNN accuracy in the estimation of the natural frequency. The next relation explained MSE as the mean of the squared difference between the foreseen frequency and expected one (Cao *et al*. 2020, Gao *et al*. 2020a, Ghabussi *et al*. 2020a, 2021, Ma *et al*. 2021, Morasaei *et al*. 2021).

$$\text{MSE}=\frac{1}{n}\sum_{i=1}^{n}\left(\text{Y-}\hat{\text{Y}}\right)^2. \tag{34}$$

5.1 ADADELTA optimizer to tune the DNN factors

ADADELTA could be selected as the optimization technique to discover decent biases and weights for minimizing the MSE. The key ADADELTA advantages have been listed below:

- This technique automatically sets the learning rate
- ADADELTA would not sensitive to the amounts of the hyperparameters
- This technique would be able to be used in distributed environments along with the local ones

To upgrade the neural network factors (weights and biases) at all iteration steps (epoch), one would employ the next equation

$$\begin{aligned} \hbar_{t+1} &= \hbar_t + \triangle \hbar_t \\ \triangle \chi_t &= -\eta \frac{\partial f(\chi_t)}{\partial \chi_t} \end{aligned} \tag{35}$$

here, η denotes the primary learning rate. For simplifying indicating the gradient of the involved factors at the t^{th} epoch, we employ G_t in place of $\frac{\partial f(\hbar_t)}{\partial \hbar_t}$. To achieve the updated weights and biases, it is needed to compute the gradient root mean square at the provided epoch by next equation

$$RMS[\Re_t] = \sqrt{E[\Re_t^2] + \varepsilon} \tag{36}$$

where, ε would be a constant. It must be implied that $E[\Re_t^2]$ indicates the expected amount of the squared gradient which would be achieved due to the subsequent definition

$$E[\Re_t^2[]\, E[\Re_{t-1}^2[](1-\rho)_t^2]] \tag{37}$$

here, ρ implies the decay rate. applying Eq. (36) and Eq. (37), one would acquire the update of the implied factors as below

$$\triangle \hbar \frac{\eta}{RMS[\Re_t[]]_{t_t}} \tag{38}$$

To wrap it up, the needed steps to discover the optimum amounts of the factors, next pseudo-code is given as Table. 1. To contrast the ADADELTA performance with other optimization techniques, Ref. (Guo *et al*. 2021) investigated their error in classifying the MNIST dataset handwriting digits for 50 epochs. As it is demonstrated in this figure, ADADELTA has a better performance rather than other optimization approaches and reaches the final amount of the error during the least number. Subsequently, ADADELTA would be classified be as one of the high-speed optimizer approach with the ability to reach the less amount of the lowest error amongst the well-known optimization techniques.

As previously implied, ADADELTA technique was employed to tune the factors of DNN to make a regression-based estimator of disk's vibration response. The hidden

Table 1 The steps required for applying ADADELTA to optimize the DNN elements (Wu 2021)

calculating updated ADADELTA at time t
requirement: consider the amounts of ρ and ε factors, suppose $\hbar_t$
1: Initialize accumulation variables $E\,[\Re^2]_0 = 0, E\,[\Delta\hbar^2]_0 = 0$
2: for t= 1 :T do %% Loop over # of updates
3: calculate Gradient: $\Re_L$
4: Accumulate Gradient: $E\,[\Re^2]_t = \rho E\,[\Re^2]_{t-1} + (1-\rho)\Re_t^2$
5: calculate Update:$\Delta x_t = -\frac{RMS[\Delta\hbar]_{t-1}}{RMS[\Re]_t}\Re_t$
6: Accumulate Updates:$E[\Delta\hbar^2]_t = \rho E[\Delta\hbar^2]_{t-1} + (1-\rho)\Delta\hbar_t^2$
7: Employ Update:$\hbar_{t+1} = \hbar_t + \Delta\hbar_t$
8: end for loop

Table 2 Material characteristics and GPLs' efficiency factor of concrete matrix

Graphene platelets (Shahverdi *et al.* 2019)	E^{GPL}[Gpa]1010	ν^{GPL}0.186	$\rho^{GPL}\left[\frac{kg}{m^3}\right]$1062..	l^{GPL}[μm] 2.5	t^{GPL}[nm] 1.5	w^{GPL}[μm] 1.5
Concrete matrix	E^m[Gpa]25	ν^m0.2	$\rho^m\left[\frac{kg}{m^3}\right]$2300			
Core aluminum	E^s[Gpa]70	ν^s0.34	$\rho^s\left[\frac{kg}{m^3}\right]$2700			
Relaxation time	$10^{-5}[s]$					

Table 3 Contrasting achieved dynamics for multifarious *h/Ro* with the outcome of Ref (Han and Liew 1999)

h/R_o	Mode number=1 (Ref (Han and Liew 1999))	Mode number=1 (Present)	Mode number=2 (Ref (Han and Liew 1999))	Mode number=2 (Present)	Mode number=3 (Ref (Han and Liew 1999))	Mode number=3 (Present)	Mode number=4 (Ref (Han and Liew 1999))	Mode number=4 (Present)
0.001	27.280	27.621156	75.364	76.137500	148.21	149.25865	245.47	246.72681
0.05	26.534	27.139571	71.228	71.934144	135.24	138.23412	215.08	218.86644
0.1	24.629	25.471425	62.140	61.888783	111.12	113.50531	167.16	169.44431
0.15	22.230	22.903314	52.762	52.671618	90.286	93.677721	131.35	132.25517

Table 4 Contrasting the first six frequencies (Hz) of the annular isotropic plate (E = 200 GPa, = 0.3, = 7850 Kg/m^3, R_0 = 125 mm, R_i = 20 mm, and h = 2 mm).

Mode number	Experimental (Alimirzaei *et al*. 2019)	Numerical (Alimirzaei *et al*. 2019)	Present study
1	168.782	163.684	162.75
2	280.974	268.845	268.23
3	399.645	389.479	388.95
4	633.833	629.471	629.12
5	705.598	683.921	683.75
6	982.243	1048.23	1047.95

layers' activation function behaves regarding Rectified linear unit (ReLU). The procedure of training is conducted by applying the 70% of the dataset. The results accuracy has been evaluated by investigating the MSE of the validation and testing dataset section. The geometrical and mechanical properties of the matrix and reinforcement have been illustrated in Table 2.

To evaluate the accuracy and validity of the provided research's approaches and techniques, calculational results have been compared with those of Ref. (Han and Liew 1999) in Table 3 in the case of the circular isotropic plate. Then, the decent agreement has been reported by the table, implying that the maximum discrepancy between the outcomes has been foreseen about 1%. Moreover, it has been seen that the frequency tended to raise by soaring up the number of modes, while the implied phenomena is likely to be reversed by adding the amount of h/R_o. So, increasing h/R_o value would lead to a drop in the frequency.

The disk's first six frequencies would be achieved and listed in Table 4 and contrasted with those determined from the computational and experimental outcomes (Alimirzaei and Mohammadimehr *et al*. 2019) with the current research. As it would be clear, the outcomes are in a desirable agreement with those achieved by the provided research.

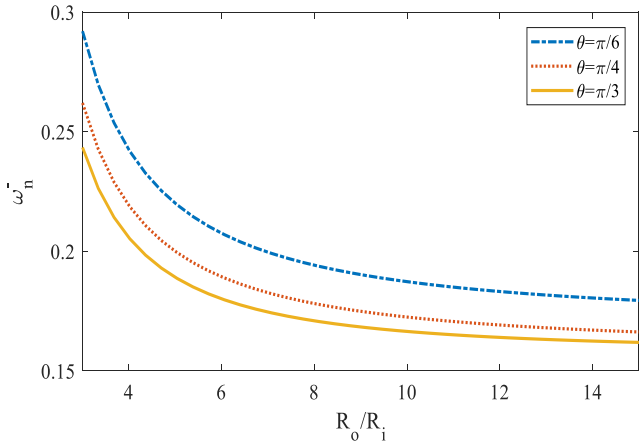

Fig. 4 Viscoelastic sandwich disk's frequency response with respect to R_o/R_i for three θ with $R_i = 200mm$, $h_H = 0.05R_i$, P = 0, $\frac{t_m}{l_m} = 0.01$, $\frac{h_m}{l_m} = 0.2$, $\Lambda_{GPL} = 0.1\ (wt\%)$, and $\frac{h_H}{h_t} = 10$

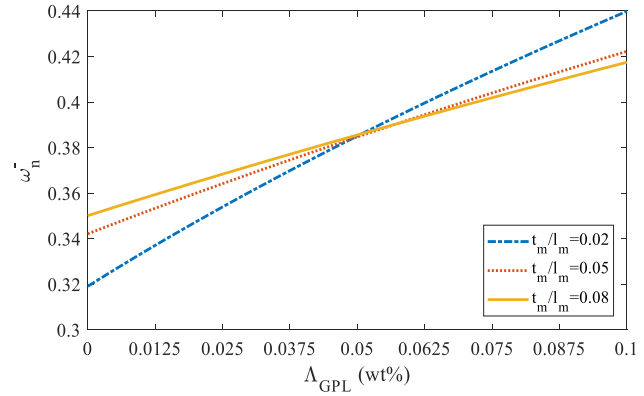

Fig. 5 Sandwich viscoelastic disk's frequency response with respect to Λ_{GPL} for three t_m/l_m with $R_i = 200mm$, $h_H = 0.05R_i$, $\frac{R_o}{R_i} = 2$, P = 0, $\frac{h_m}{l_m} = 0.2$, $\frac{h_H}{h_t} = 10$, $\theta = \frac{\pi}{4}$

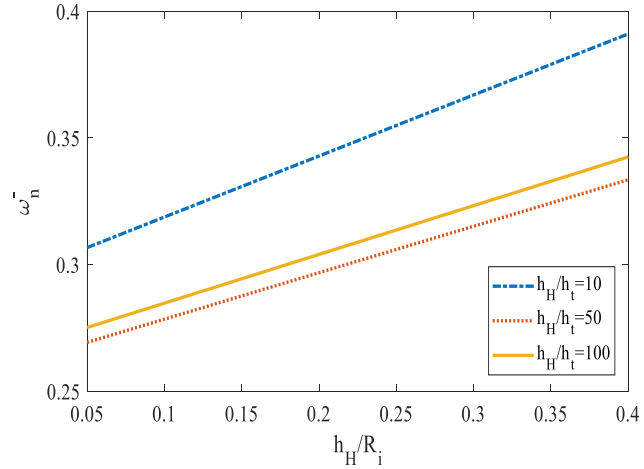

Fig. 6 Sandwich viscoelastic disk's frequency response with respect to h_H/R_i for three h_H/h_t with $R_i = 200mm$, $\frac{R_o}{R_i} = 2$, P = 0, $\frac{t_m}{l_m} = 0.01$, $\frac{h_m}{l_m} = 0.2$, $\Lambda_{GPL} = 0.1\ (wt\%)$, and $\theta = \frac{\pi}{4}$

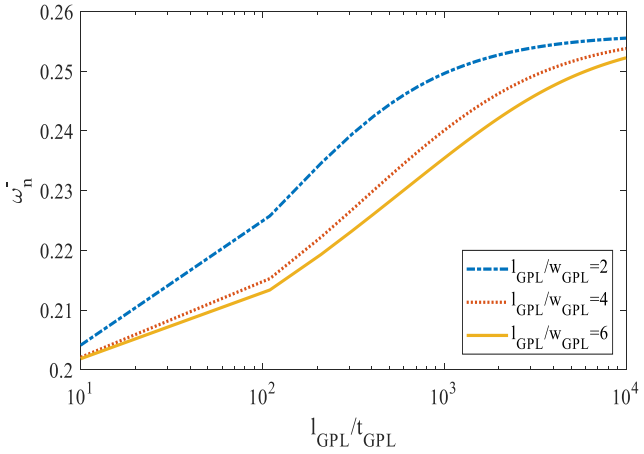

Fig. 7 Sandwich viscoelastic disk's frequency response with respect to l_{GPL}/t_{GPL} for three l_{GPL}/w_{GPL} with $R_i = 200mm$, $h_H = 0.05R_i$, $\frac{R_o}{R_i} = 2$, P = 0, $\frac{t_m}{l_m} = 0.01$, $\frac{h_m}{l_m} = 0.2$, $\frac{h_H}{h_t} = 10$, $\Lambda_{GPL} = 0.1\ (wt\%)$, and $\theta = \frac{\pi}{4}$

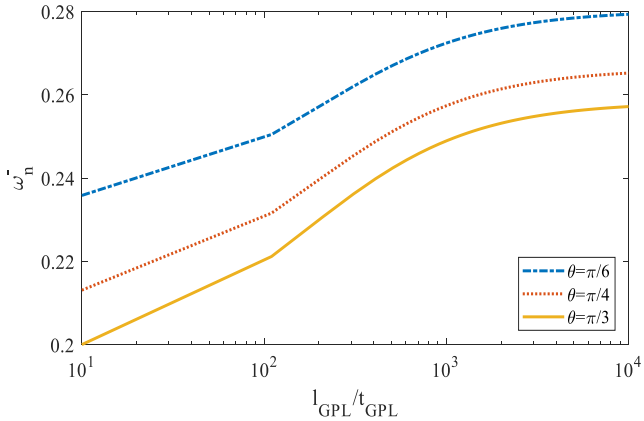

Fig. 8 The sandwich viscoelastic disk's frequency response with respect to l_{GPL}/t_{GPL} for three θ with $R_i = 200mm$, $h_H = 0.05R_i$, $\frac{R_o}{R_i} = 2$, P = 0, $\frac{t_m}{l_m} = 0.01$, $\frac{h_m}{l_m} = 0.2$, $\Lambda_{GPL} = 0.1\ (wt\%)$, and $\frac{h_H}{h_t} = 10$

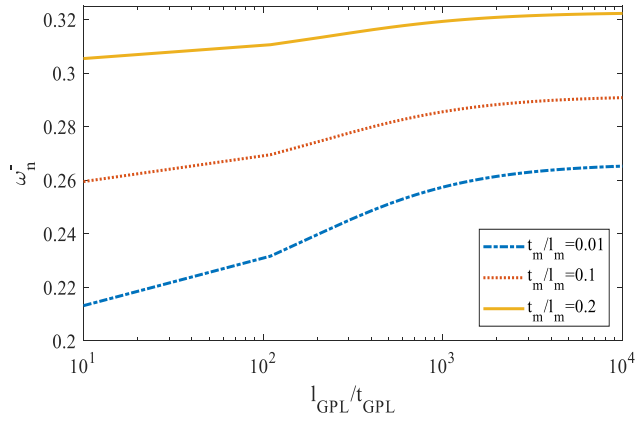

Fig. 9 The sandwich viscoelastic disk's frequency response respect to l_{GPL}/t_{GPL} for three t_m/l_m with $R_i = 200mm$, $h_H = 0.05R_i$, $\frac{R_o}{R_i} = 2$, P = 0, $\frac{h_m}{l_m} = 0.2$, $\frac{h_H}{h_t} = 10$, $\Lambda_{GPL} = 0.1\ (wt\%)$, and $\theta = \frac{\pi}{4}$

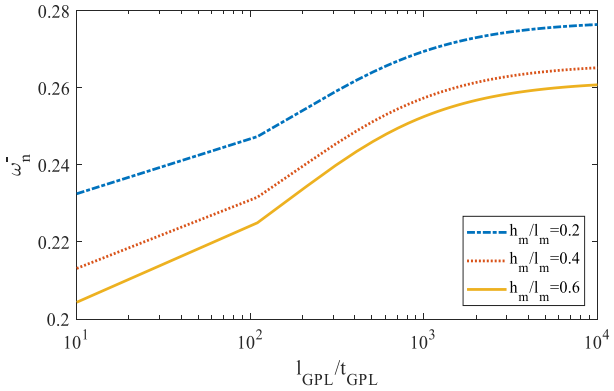

Fig. 10 The sandwich viscoelastic disk's frequency response of the respect to l_{GPL}/t_{GPL} for three h_m/l_m with $R_i = 200mm$, $h_H = 0.05R_i$, $\frac{R_o}{R_i} = 2$, P = 0, $\frac{t_m}{l_m} = 0.01$, $\frac{h_H}{h_t} = 10$, $\Lambda_{GPL} = 0.1\ (wt\%)$, and $\theta = \frac{\pi}{4}$

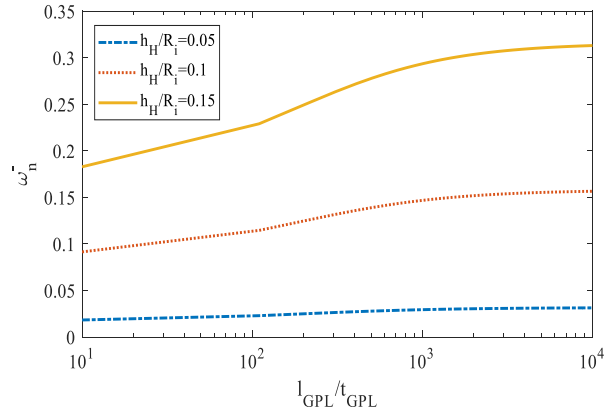

Fig. 11 sandwich viscoelastic disk's frequency response respect to l_{GPL}/t_{GPL} for three h_H/R_i with $R_i = 200mm$, $\frac{R_o}{R_i} = 2$, P = 0, $\frac{t_m}{l_m} = 0.01$, $\frac{h_m}{l_m} = 0.2$, $\frac{h_H}{h_t} = 10$, $\Lambda_{GPL} = 0.1\ (wt\%)$, and $\theta = \frac{\pi}{4}$

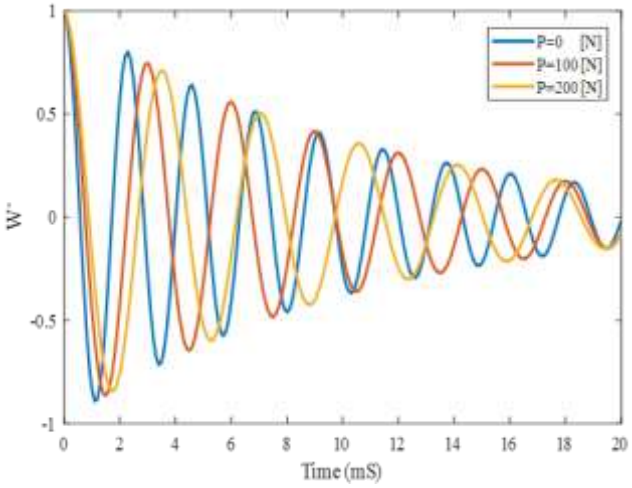

Fig. 12 deflection and Time history of the viscoelastic sandwich system with attention to the natural residual pressure's influence with $R_i = 200mm$, $h_H = 0.05R_i$, $\frac{R_o}{R_i} = 2$, $\frac{t_m}{l_m} = 0.01$, $\frac{h_m}{l_m} = 0.2$, $\frac{h_H}{h_t} = 10$, $\Lambda_{GPL} = 0.1\ (wt\%)$, and $\theta = \frac{\pi}{4}$

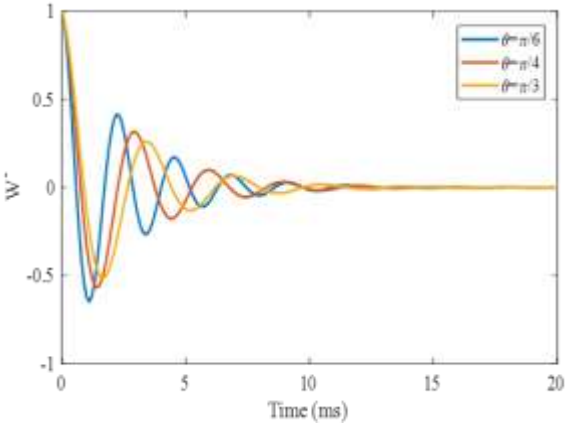

Fig. 13 sandwich viscoelastic disk's deflection and Time history of the with attention to the influence of fibers angel with $R_i = 200mm$, $h_H = 0.05R_i$, $\frac{R_o}{R_i} = 2$, P=0, $\frac{t_m}{l_m} = 0.01$, $\frac{h_m}{l_m} = 0.2$, $\Lambda_{GPL} = 0.1\ (wt\%)$, and $\frac{h_H}{h_t} = 10$

6. Numerical results

Research on the sandwich viscoelastic disk's frequency response considering honeycomb core and FG-GPLRVC face sheets taking into account the impact of the angel of honeycomb core in Fig. 4. Moreover, for the angle of below $\pi/3$, with raise in θ the disk's stability faces with a drop while for the angle would be more than $\pi/3$, there is an enhancement in the sandwich viscoelastic disk's dynamics. A presentation on the sandwich viscoelastic disk's frequency response considering the influence of weight fraction of GPLs (Λ_{GPL}) and thickness to length ratio (t_m/l_m) is proved in Fig. 5. The most highlighted outcome in this step is that the influence of t_m/l_m on the sandwich viscoelastic disk's frequency of the considering FG-GPLRVC face sheets and honeycomb core has highly dependent on Λ_{GPL}. In order to create a comprehensive definition should imply that for primary amounts of Λ_{GPL}, raising t_m/l_mwould be a reason to boost the disk's natural frequency while raising the reinforcement percentage in the epoxy matrix and after a specific value of Λ_{GPL}, system's stability response would be declined when the Λ_{GPL} factor raises.

A presentation on the sandwich viscoelastic disk's frequency response taking into consideration the influences of the honeycomb core to thickness ratio of FG face sheet (h_H/h_t) and thickness of honeycomb core to internal radius ratio (h_H/R_i) is provided in Fig. 6. Commonly, for all amounts of h_H/h_t, raising the h_H/R_i could boost the sandwich viscoelastic disk's dynamics, linearly. For simply-simply ends, as honeycomb core's thickness increases, we would be facing better dynamic performance in the system, however, this enhancement would be weak at higher h_H/h_t.

To scrutinize the sandwich viscoelastic disk's frequency response considering FG-GPLRVC face sheets and honeycomb core regarding influences of the honeycomb core on the ratio thickness of FG face sheet (h_H/h_t) and ratio of honeycomb core thickness to internal radius (h_H/R_i) has been provided in Fig. 7. If the system is filled with the

Table 5 DNN's estimation performance of the model with respect to training data with $R_i = 200mm$, $\frac{R_o}{R_i} = 2$, P=0, $\frac{t_m}{l_m} = 0.01$, $\frac{h_m}{l_m} = 0.2$, $\Lambda_{GPL} = 0.1\ (wt\%)$, and $\theta = \frac{\pi}{4}$

$\frac{h_H}{h_t} = 10$				
		Predicted		
$\frac{h_H}{R_i}$	Fit	$MSE_{Train} = 0.09 \times 10^{-6}$	$MSE_{Train} = 0.15 \times 10^{-6}$	$MSE_{Train} = 0.45 \times 10^{-6}$
0.05	0.3061	0.3525	0.3132	0.3085
0.1	0.3186	0.2673	0.3012	0.3123
0.15	0.3303	0.2821	0.3142	0.3291
0.2	0.3424	0.4175	0.3546	0.3473
0.25	0.3545	0.2923	0.3452	0.3512
0.3	0.3666	0.3894	0.3723	0.3673
0.35	0.3787	0.3154	0.3652	0.3745
0.4	0.3908	0.4721	0.4012	0.3991
$\frac{h_H}{h_t} = 50$				
0.05	0.2691	0.1985	0.2541	0.2612
0.1	0.2782	0.3121	0.2875	0.2799
0.15	0.2878	0.3212	0.2963	0.2901
0.2	0.2962	0.2432	0.2863	0.2941
0.25	0.3057	0.3512	0.3112	0.3061
0.3	0.3145	0.3011	0.3095	0.3101
0.35	0.3241	0.3921	0.3345	0.3291
0.4	0.3332	0.3541	0.3412	0.3341

wither and thicker GPLs, the porous sandwich disk's frequency will be decreasing and boosting, respectively. By a precise looking at Fig. 8 it would be clear that in the case of longer GPLs, the impacts of the thickness width and of the filler on the frequency drops.

An analysis on the sandwich viscoelastic disk's frequency response considering FG-GPLRVC face sheets and honeycomb core regarding the effects of honeycomb core angle (θ) and the l_{GPL}/t_{GPL} would be provided in Fig. 8.

A study on the viscoelastic sandwich disk's frequency considering honeycomb core regarding the influences of the l_{GPL}/t_{GPL} and t_m/l_m is presented in Fig. 9. For the below figure could be reported that using the longer GPLs provides an improvement on the stability of the viscoelastic sandwich system.

The sandwich porous disk's frequency response considering honeycomb core has been analyzed in Fig. 10 regarding influences of the h_m/l_m and l_{GPL}/t_{GPL}. By attention to Fig. 10 would be implied that there would be an improvement in the sandwich porous system's stability considering a raise in the l_{GPL}/t_{GPL} and a drop in the h_m/l_m.

Fig. 11 investigates the dynamics of the sandwich viscoelastic disk by considering h_H/R_i and l_{GPL}/t_{GPL} influences. In addition to enhancing the dynamics due to a drop in the h_H/R_i, the sandwich disk's frequency would be boosted by applying the thinner GPLs.

Scrutinize on the time history of the sandwich disk by considering the internal pressure p impact on the system's deflection, which is reported in Fig. 12. Accordingly, as the internal pressure enhances, the time domain rises but the system's deflection drops. So, when the internal pressure increases, providing a stable condition needs more time.

The provided diagrams in Fig.13 create an investigation on sandwich viscoelastic disk's deflection and the time history regarding the influence of fibers angle. Through Fig.13, the structure's stability would be created in less time, as long as the fibers in the matrix distribute vertically. Moreover, for all time domains, as the fibers angle raises, the system's deflection declines.

The training process outcomes are illustrated in Table 5. Regarding this table, the nuance between the estimated dimensionless frequencies and the expected ones are highly acceptable for various $\frac{h_H}{R_i}$ and $\frac{h_H}{h_t}$. Since the estimated points have a little distance from the solid line. The training procedure's small MSE ($MSE_{Train} = 0.09 * 10^{-6}$) denotes the superb abilities of ADADELTA to discover the decent factors to tune the DNN. To mentioned fully connected DNN's astonishing performance to be reliable, it would be needed to analyze the approach accuracy toward test and validation sets. Due to the given table, the nuance between the thought frequencies and the estimated ones would be reasonable desirable. Because the estimated points have a little distance from the solid line. The test procedure's small MSE ($MSE_{Test} = 0.45 * 10^{-6}$) denotes the strength of the mentioned technique to estimate the system's vibration. It

can be concluded that by increasing the MSE_{Test} value, the results are close to the actual outcomes.

7. Conclusions

Sandwich viscoelastic disk's vibrational characteristics considering GPLRVC face sheets and honeycomb core with concrete matrix via deep learning had been analyzed. The optimum values of the parameters involved in the fully connected neural network had been determined through the momentum-based optimizer. The strength of the method applied in this study came from the high accuracy besides lower epochs needed to train the multi-layered network. The strains and stresses were achieved employing FSDT. Modified Halpin–Tsai and mixture Rule model are involved in creating the efficient graphene nano-platelets face sheets' material constant of the viscoelastic sandwich disk. Ultimately, the most highlighted outcomes of this research would be as below:

• The system's stability would be created in less time, as long as the matrix fibers distribute vertically. Moreover, for all time domains, as the angel of fibers and internal pressure raise, the system deflection would be declined.

• The relation between frequency characteristics and R_o/R_i of the sandwich, viscoelastic disk considering FG face sheet and honeycomb core has considerable dependence on the angle of honeycomb core.

• For h_H/h_t values of below 30, if we raise the h_H/h_t, the frequency decreases, however, this system's behavior would be boosted for h_H/h_t higher than 30.

• As the GPLs are wider, more frequency has been observed specifically at the primary l_{GPL}/t_{GPL}.

• By increasing the MSE_{Test} value, the results are close to the actual outcomes.

References

Al-Furjan, M., Habibi, M., Ghabussi, A., Safarpour, H., Safarpour, M. and Tounsi, A. (2020), "Non-polynomial framework for stress and strain response of the FG-GPLRC disk using three-dimensional refined higher-order theory", *Eng. Struct.*, **228**, 111496. https://doi.org/10.1016/j.engstruct.2020.111496.

Alimirzaei, S., Mohammadimehr, M. and Tounsi, A. (2019), "Nonlinear analysis of viscoelastic micro-composite beam with geometrical imperfection using FEM: MSGT electro-magneto-elastic bending, buckling and vibration solutions", *Struct. Eng. Mech.* **71**(5), 485-502. https://doi.org/10.12989/sem.2019.71.5.485.

Alipour, M., Torabi, M.A., Sareban, M., Lashini, H., Sadeghi, E., Fazaeli, A., Habibi, M. and Hashemi, R. (2020), "Finite element and experimental method for analyzing the effects of martensite morphologies on the formability of DP steels", *Mech. Based Des. Struct.*, **48**(5), 525-541. https://doi.org/10.1080/15397734.2019.1633343.

Allam, O., Draiche, K., Bousahla, A.A., Bourada, F., Tounsi, A., Benrahou, K.H., Mahmoud, S., Adda Bedia, E. and Tounsi, A. (2020), "A generalized 4-unknown refined theory for bending and free vibration analysis of laminated composite and sandwich plates and shells", *Comput. Concrete*, **26**(2), 185-201. http://doi.org/10.12989/cac.2020.26.2.185.

Amini, A., Mohammadimehr, M. and Faraji, A. (2019), "Active control to reduce the vibration amplitude of the solar honeycomb sandwich panels with CNTRC facesheets using piezoelectric patch sensor and actuator", *Steel Compos. Struct.*, **32**(5), 671-686. https://doi.org/10.12989/scs.2019.32.5.671.

Ansari, R. and Torabi, J. (2019), "Semi-analytical postbuckling analysis of polymer nanocomposite cylindrical shells reinforced with functionally graded graphene platelets", *Thin Wall. Struct.*, **144**, 106248. https://doi.org/10.1016/j.tws.2019.106248.

Bourada, F., Bousahla, A.A., Tounsi, A., Bedia, E., Mahmoud, S., Benrahou, K.H. and Tounsi, A. (2020), "Stability and dynamic analyses of SW-CNT reinforced concrete beam resting on elastic-foundation", *Comput. Concrete*, **25**(6), 485-495, https://doi.org/10.12989/cac.2020.25.6.485.

Cai, X., Zhong, S., Wang, J. and Shi, K. (2020), "Robust H∞ control for uncertain delayed TS fuzzy systems with stochastic packet dropouts", *Appl. Math. Comput.*, **385**, 125432. https://doi.org/10.1016/j.amc.2020.125432

Cai, K., Chen, H., Ai, W., Miao, X., Lin, Q. and Feng, Q. (2021a), "Feedback convolutional network for intelligent data fusion based on near-infrared collaborative IoT technology", *IEEE T. Ind. Inform.*, **18**(2). https://doi.org/10.1109/TII.2021.3076513.

Cai, X., Shi, K., Zhong, S. and Pang, X. (2021b), "Dissipative sampled-data control for high-speed train systems with quantized measurements", *IEEE T Intell. Transp.* https://doi.org/10.1109/TITS.2021.3052940.

Cai, X., Shi, K., Zhong, S., Wang, J. and Tang, Y. (2021c), "Dissipative analysis for high speed train systems via looped-functional and relaxed condition methods", *Appl. Math. Model.*, **96**, 570-583. https://doi.org/10.1016/j.apm.2021.03.042.

Cao, Y., Miraba, S., Rafiei, S., Ghabussi, A., Bokaei, F., Baharom, S., Haramipour, P. and Assilzadeh, H. (2020), "Economic application of structural health monitoring and internet of things in efficiency of building information modeling", *Smart Struct. Syst.*, **26**(5), 559-573, https://doi.org/10.12989/sss.2020.26.5.559.

Dai, H. and Safarpour, H. (2021), "Frequency and thermal buckling information of laminated composite doubly curved open nanoshell", *Adv. Nano Res.*, **10**(1), 1-14, https://doi.org/10.12989/anr.2021.10.1.001.

Dai, Z., Jiang, Z., Zhang, L. and Habibi, M. (2021), "Frequency characteristics and sensitivity analysis of a size-dependent laminated nanoshell", *Adv. Nano Res.*, **10**(2), 175-189. https://doi.org/10.12989/anr.2021.10.2.175.

Draoui, A., Zidour, M., Tounsi, A. and Adim, B. (2019). "Static and dynamic behavior of nanotubes-reinforced sandwich plates using (FSDT)", *J. Nano Res.*, **57**, 117-135. https://doi.org/10.4028/www.scientific.net/JNanoR.57.117.

Ebrahimi, F. and Safarpour, H. (2018), "Vibration analysis of inhomogeneous nonlocal beams via a modified couple stress theory incorporating surface effects", *Wind Struct.*, **27**(6), 431-438. https://doi.org/10.12989/was.2018.27.6.431.

Ebrahimi, F., Habibi, M. and Safarpour, H. (2019a), "On modeling of wave propagation in a thermally affected GNP-reinforced imperfect nanocomposite shell", *Eng. Comput.*, **35**(4), 1375-1389. https://doi.org/10.1007/s00366-018-0669-4.

Ebrahimi, F., Hajilak, Z.E., Habibi, M. and Safarpour, H. (2019b), "Buckling and vibration characteristics of a carbon nanotube-reinforced spinning cantilever cylindrical 3D shell conveying viscous fluid flow and carrying spring-mass systems under various temperature distributions", *Proceedings of the Institution of Mechanical Engineers, Part C: Journal of Mechanical Engineering Science*. **233**(13), 4590-4605, https://doi.org/10.1177/0954406219832323.

Ebrahimi, F., Mohammadi, K., Barouti, M.M. and Habibi, M. (2019c), "Wave propagation analysis of a spinning porous graphene nanoplatelet-reinforced nanoshell", *Wave. Random Complex*, 1-27.

https://doi.org/10.1080/17455030.2019.1694729.

Ebrahimi, F., Hashemabadi, D., Habibi, M. and Safarpour, H. (2020a), "Thermal buckling and forced vibration characteristics of a porous GNP reinforced nanocomposite cylindrical shell", *Microsyst. Technol.*, **26**(2), 461-473, https://doi.org/10.1007/s00542-019-04542-9.

Ebrahimi, F., Supeni, E.E.B., Habibi, M. and Safarpour, H. (2020b), "Frequency characteristics of a GPL-reinforced composite microdisk coupled with a piezoelectric layer", *Eur. Phys. J. Plus.* **135**(2), 144, https://doi.org/10.1140/epjp/s13360-020-00217-x.

Esmailpoor Hajilak, Z., Pourghader, J., Hashemabadi, D., Sharifi Bagh, F., Habibi, M. and Safarpour, H. (2019), "Multilayer GPLRC composite cylindrical nanoshell using modified strain gradient theory", *Mech. Based Des. Struct.*, **47**(5), 521-545. https://doi/10.1080/15397734.2019.1566743.

Feng, S., Zuo, C., Zhang, L., Tao, T., Hu, Y., Yin, W., Qian, J. and Chen, Q. (2021a), "Calibration of fringe projection profilometry: A comparative review", *Opt. Laser Eng.*, **143**, 106622. https://doi.org/10.1016/j.optlaseng.2021.106622.

Feng, S., Zuo, C., Zhang, L., Yin, W. and Chen, Q. (2021b), "Generalized framework for non-sinusoidal fringe analysis using deep learning", *Photo. Res.*, **9**(6), 1084-1098. https://doi.org/10.1364/PRJ.420944.

Feng, J., Liu, Z. and Feng, L. (2021c), "Identifying opportunities for sustainable business models in manufacturing: Application of patent analysis and generative topographic mapping", *Sustain. Product. Consum.*, **27**, 509-522. https://doi.org/10.1016/j.spc.2021.01.021

Gao, N., Wei, Z., Zhang, R. and Hou, H. (2019), "Low-frequency elastic wave attenuation in a composite acoustic black hole beam", *Appl. Acoust.*, **154**, 68-76. https://doi.org/10.1016/j.apacoust.2019.04.029.

Gao, N. and Lu, K. (2020), "An underwater metamaterial for broadband acoustic absorption at low frequency", *Appl. Acoust.*, **169**, 107500. https://doi.org/10.1016/j.apacoust.2020.107500.

Gao, J., Koopialipoor, M., Armaghani, D.J., Ghabussi, A., Baharom, S., Morasaei, A., Shariati, A., Khorami, M. and Zhou, J. (2020a), "Evaluating the bond strength of FRP in concrete samples using machine learning methods", *Smart Struct. Syst.*, **26**(4), 403-418. https://doi.org/10.12989/sss.2020.26.4.403.

Gao, N., Luo, D., Cheng, B. and Hou, H. (2020b), "Teaching-learning-based optimization of a composite metastructure in the 0–10 kHz broadband sound absorption range", *J. Acoust. Soc. Am.*, **148**(2), EL125-129. https://doi.org/10.1121/10.0001678.

Gao, N., Guo, X., Deng, J., Cheng, B. and Hou, H. (2021a), "Elastic wave modulation of double-leaf ABH beam embedded mass oscillator", *Appl. Acoust.*, **173**, 107694. https://doi.org/10.1016/j.apacoust.2020.107694.

Gao, N., Tang, L., Deng, J., Lu, K., Hou, H. and Chen, K. (2021b), "Design, fabrication and sound absorption test of composite porous metamaterial with embedding I-plates into porous polyurethane sponge", *Appl. Acoust.*, **175**, 107845. https://doi.org/10.1016/j.apacoust.2020.107845.

Gao, N., Wang, B., Lu, K. and Hou, H. (2021c), "Complex band structure and evanescent Bloch wave propagation of periodic nested acoustic black hole phononic structure", *Appl. Acoust.*, **177**, 107906. https://doi.org/10.1016/j.apacoust.2020.107906.

Ghabussi, A., Ashrafi, N., Shavalipour, A., Hosseinpour, A., Habibi, M., Moayedi, H., Babaei, B. and Safarpour, H. (2019), "Free vibration analysis of an electro-elastic GPLRC cylindrical shell surrounded by viscoelastic foundation using modified length-couple stress parameter", *Mech. Based Des. Struct.*, 1-25. https://doi.org/10.1080/15397734.2019.1705166.

Ghabussi, A., Habibi, M., NoormohammadiArani, O., Shavalipour, A., Moayedi, H. and Safarpour, H. (2020a), "Frequency characteristics of a viscoelastic graphene nanoplatelet–reinforced composite circular microplate", *J. Vib. Control*, **27**(1-2), 101-118. https://doi.org/10.1177/1077546320923930.

Ghabussi, A., Marnani, J.A. and Rohanimanesh, M.S. (2020b). "Improving seismic performance of portal frame structures with steel curved dampers", *Structures*, **24**, pp. 27-40. https://doi.org/10.1016/j.istruc.2019.12.025.

Ghabussi, A., Asgari Marnani, J. and Rohanimanesh, M.S. (2021), "Seismic performance assessment of a novel ductile steel braced frame equipped with steel curved damper", *Structures*, **31**, 87-97. https://doi.org/10.1016/j.istruc.2021.01.073.

Ghavanloo, E. and Fazelzadeh, S.A. (2011), "Flow-thermoelastic vibration and instability analysis of viscoelastic carbon nanotubes embedded in viscous fluid", *Physica E*, **44**(1), 17-24. https://doi.org/10.1016/j.physe.2011.06.024.

Ghazanfari, A., Soleimani, S.S., Keshavarzzadeh, M., Habibi, M., Assempuor, A. and Hashemi, R. (2020), "Prediction of FLD for sheet metal by considering through-thickness shear stresses", *Mech. Based Des. Struct.*, **48**(6), 755-772. https://doi.org/10.1080/15397734.2019.1662310.

Gibson, L.J. and Ashby, M.F. (1999), *Cellular Solids: Structure and Properties*, Cambridge University Press, Cambridge, U.K.

Gong, C., Hu, Y., Gao, J., Wang, Y. and Yan, L. (2019), "An improved delay-suppressed sliding-mode observer for sensorless vector-controlled PMSM", *IEEE T Ind. Electron.*, **67**(7), 5913-5923. https://doi.org/10.1109/TIE.2019.2952824.

Gunasekaran, V., Pitchaimani, J. and Chinnapandi, L.B.M. (2020), "Analytical investigation on free vibration frequencies of polymer nano composite plate: Effect of graphene grading and non-uniform edge loading", *Mater. Today Commun.*, **24**, 100910. https://doi.org/10.1016/j.mtcomm.2020.100910.

Guo, J., Baharvand, A., Tazeddinova, D., Habibi, M., Safarpour, H., Roco-Videla, A. and Selmi, A. (2021), "An intelligent computer method for vibration responses of the spinning multi-layer symmetric nanosystem using multi-physics modeling", *Eng. Comput.*, 1-22. https://doi.org/10.1007/s00366-021-01433-4.

Habibi, M., Hashemi, R., Sadeghi, E., Fazaeli, A., Ghazanfari, A. and Lashini, H. (2016), "Enhancing the mechanical properties and formability of low carbon steel with dual-phase microstructures", *J. Mater. Eng. Perform.*, **25**(2), 382-389. https://doi.org/10.1007/s11665-016-1882-1.

Habibi, M., Ghazanfari, A., Assempour, A., Naghdabadi, R. and Hashemi, R. (2017), "Determination of forming limit diagram using two modified finite element models", *Mech Eng.* **48**(4), 141-144. https://doi.org/10.22060/MEJ.2016.664.

Habibi, M., Hashemi, R., Ghazanfari, A., Naghdabadi, R. and Assempour, A. (2018a), "Forming limit diagrams by including the M–K model in finite element simulation considering the effect of bending", *Proceedings of the Institution of Mechanical Engineers, Part L: Journal of Materials: Design and Applications*. **232**(8), 625-636. https://doi.org/10.1177/1464420716642258.

Habibi, M., Hashemi, R., Tafti, M.F. and Assempour, A. (2018b), "Experimental investigation of mechanical properties, formability and forming limit diagrams for tailor-welded blanks produced by friction stir welding", *J. Manuf. Proc.*, **31**, 310-323. https://doi.org/10.1016/j.jmapro.2017.11.009.

Habibi, M., Hashemabadi, D. and Safarpour, H. (2019a), "Vibration analysis of a high-speed rotating GPLRC nano-structure coupled with a piezoelectric actuator", *Eur. Phys. J. Plus*, **134**(6), 307. https://doi.org/10.1140/epjp/i2019-12742-7.

Habibi, M., Mohammadgholiha, M. and Safarpour, H. (2019b), "Wave propagation characteristics of the electrically GNP-reinforced nanocomposite cylindrical shell", *J. Braz. Soc. Mech. Sci. Eng.*, **41**(5), 221. https://doi.org/10.1007/s40430-019-1715-x.

Habibi, M., Mohammadi, A., Safarpour, H. and Ghadiri, M.

(2019c), "Effect of porosity on buckling and vibrational characteristics of the imperfect GPLRC composite nanoshell", *Mech. Based Des. Struct.*, 1-30, https://doi.org/10.1080/15397734.2019.1701490.

Habibi, M., Mohammadi, A., Safarpour, H., Shavalipour, A. and Ghadiri, M. (2019d), "Wave propagation analysis of the laminated cylindrical nanoshell coupled with a piezoelectric actuator", *Mech. Based Des. Struct.*, 1-19, https://doi.org/10.1080/15397734.2019.1697932.

Habibi, M., Taghdir, A. and Safarpour, H. (2019e), "Stability analysis of an electrically cylindrical nanoshell reinforced with graphene nanoplatelets", *Composites Part B Eng.*, **175** 107125, https://doi.org/10.1016/j.compositesb.2019.107125.

Habibi, M., Safarpour, M. and Safarpour, H. (2020), "Vibrational characteristics of a FG-GPLRC viscoelastic thick annular plate using fourth-order Runge-Kutta and GDQ methods", *Mech. Based Des. Struct.*, 1-22, https://doi.org/10.1080/15397734.2020.1779086.

Habibi, M., Darabi, R., Sa, J.C.d. and Reis, A. (2021), "An innovation in finite element simulation via crystal plasticity assessment of grain morphology effect on sheet metal formability", *Proceedings of the Institution of Mechanical Engineers, Part L: Journal of Materials: Design and Applications*. **235**(8), 1937-1951. https://doi.org/10.1177/14644207211024686.

Han, J.B. and Liew, K. (1999), "Axisymmetric free vibration of thick annular plates", *Int. J. Mech. Sci.*, **41**(9), 1089-1109, https://doi.org/10.1016/S0020-7403(98)00057-5.

Han, X., Chen, N., Yan, J., Liu, J., Liu, M. and Karellas, S. (2019), "Thermodynamic analysis and life cycle assessment of supercritical pulverized coal-fired power plant integrated with No. 0 feedwater pre-heater under partial loads", *J. Clean. Prod.*, **233**, 1106-1122. https://doi.org/10.1016/j.jclepro.2019.06.159

Han, X., Wei, Z., Zhang, B., Li, Y., Du, T. and Chen, H. (2021), "Crop evapotranspiration prediction by considering dynamic change of crop coefficient and the precipitation effect in back-propagation neural network model", *J. Hydrol.*, **596** 126104. https://doi.org/10.1016/j.jhydrol.2021.126104

Hashemi, H.R., Alizadeh, A.a., Oyarhossein, M.A., Shavalipour, A., Makkiabadi, M. and Habibi, M. (2019), "Influence of imperfection on amplitude and resonance frequency of a reinforcement compositionally graded nanostructure", *Wave. Random Complex*, 1-27, https://doi.org/10.1080/17455030.2019.1662968.

He, Y., Dai, L. and Zhang, H. (2020), "Multi-branch deep residual learning for clustering and beamforming in user-centric Network", *IEEE Commun. Lett.*, **24**(10), 2221-2225. https://doi.org/10.1109/LCOMM.2020.3005947.

He, X., Ding, J., Habibi, M., Safarpour, H. and Safarpour, M. (2021), "Non-polynomial framework for bending responses of the multi-scale hybrid laminated nanocomposite reinforced circular/annular plate", *Thin Wall. Struct.*, **166** 108019. https://doi.org/10.1016/j.tws.2021.108019.

Hou, F., Wu, S., Moradi, Z. and Shafiei, N. (2021), "The computational modeling for the static analysis of axially functionally graded micro-cylindrical imperfect beam applying the computer simulation", *Eng. Comput.*, 1-19, https://doi.org/10.1007/s00366-021-01456-x.

Hu, P., Cao, L., Su, J., Li, Q. and Li, Y. (2020), "Distribution characteristics of salt-out particles in steam turbine stage", *Energy*, **192**, 116626. https://doi.org/10.1016/j.energy.2019.116626

Huang, X., Hao, H., Oslub, K., Habibi, M. and Tounsi, A. (2021a), "Dynamic stability/instability simulation of the rotary size-dependent functionally graded microsystem", *Eng. Comput.*,1-17. https://doi.org/10.1007/s00366-021-01399-3.

Huang, X., Zhang, Y., Moradi, Z. and Shafiei, N. (2021b), "Computer simulation via a couple of homotopy perturbation methods and the generalized differential quadrature method for nonlinear vibration of functionally graded non-uniform micro-tube", *Eng. Comput.*, 1-18. https://doi.org/10.1007/s00366-021-01395-7.

Huang, X., Zhu, Y., Vafaei, P., Moradi, Z. and Davoudi, M. (2021c), "An iterative simulation algorithm for large oscillation of the applicable 2D-electrical system on a complex nonlinear substrate", *Eng. Comput.*, 1-13. https://doi.org/10.1007/s00366-021-01320-y.

Huo, J., Zhang, G., Ghabussi, A. and Habibi, M. (2021), "Bending analysis of FG-GPLRC axisymmetric circular/annular sector plates by considering elastic foundation and horizontal friction force using 3D-poroelasticity theory", *Compos. Struct.*, **276**, 114438. https://doi.org/10.1016/j.compstruct.2021.114438.

Javani, M., Kiani, Y. and Eslami, M. (2020), "Thermal buckling of FG graphene platelet reinforced composite annular sector plates", *Thin Wall. Struct.*, **148**, 106589, https://doi.org/10.1016/j.tws.2019.106589.

Jermsittiparsert, K., Ghabussi, A., Forooghi, A., Shavalipour, A., Habibi, M., won Jung, D. and Safa, M. (2020), "Critical voltage, thermal buckling and frequency characteristics of a thermally affected GPL reinforced composite microdisk covered with piezoelectric actuator", *Mech. Based Des. Struct.*, 1-23, https://doi.org/10.1080/15397734.2020.1748052.

Jiang, L., Zhang, B., Han, S., Chen, H. and Wei, Z. (2021), "Upscaling evapotranspiration from the instantaneous to the daily time scale: Assessing six methods including an optimized coefficient based on worldwide eddy covariance flux network", *J. Hydrol.*, **596**, 126135. https://doi.org/10.1016/j.jhydrol.2021.126135

Jiao, J., Ghoreishi, S.M., Moradi, Z. and Oslub, K. (2021), "Coupled particle swarm optimization method with genetic algorithm for the static–dynamic performance of the magneto-electro-elastic nanosystem", *Eng. Comput.*, https://doi.org/10.1007/s00366-021-01391-x.

Khosravi, F. and Hosseini, S.A. (2020), "On the viscoelastic carbon nanotube mass nanosensor using torsional forced vibration and Eringen's nonlocal model", *Mech. Based Des. Struct.*, 1-24. https://doi.org/10.1080/15397734.2020.1744001.

Khosravi, F., Hosseini, S.A. and Tounsi, A. (2020), "Torsional dynamic response of viscoelastic SWCNT subjected to linear and harmonic torques with general boundary conditions via Eringen's nonlocal differential model", *Eur. Phys. J. Plus.*, **135**(2), 183. https://doi.org/10.1016/j.measurement.2020.108026.

Li, B., Xiao, G., Lu, R., Deng, R. and Bao, H. (2019), "On feasibility and limitations of detecting false data injection attacks on power grid state estimation using D-FACTS devices", *IEEE T. Ind. Inform.*, **16**(2), 854-864. https://doi.org/10.1109/ACCESS.2020.2999585.

Li, B., Wu, Y., Song, J., Lu, R., Li, T. and Zhao, L. (2020), "DeepFed: Federated Deep Learning for Intrusion Detection in Industrial Cyber–Physical Systems", *IEEE T. Ind. Inform.*, **17**(8), 5615-5624. https://doi.org/10.1109/TII.2020.3023430.

Li, B., Liang, R., Zhou, W., Yin, H., Gao, H. and Cai, K. (2021a), "LBS meets blockchain: an efficient method with security preserving trust in SAGIN", *IEEE Internet Thing J.* https://doi.org/10.1109/JIOT.2021.3064357

Li, X., Dong, Z.Q., Yu, P., Wang, L.P., Niu, X.D., Yamaguchi, H. and Li, D.C. (2021b), "Effect of self-assembly on fluorescence in magnetic multiphase flows and its application on the novel detection for COVID-19", *Phys. Fluid.*, **33**(4), 042004. https://doi.org/10.1063/5.0048123.

Liu, D., Li, Z., Kitipornchai, S. and Yang, J. (2019), "Three-dimensional free vibration and bending analyses of functionally graded graphene nanoplatelets-reinforced nanocomposite

annular plates", *Compos. Struct.*, **229**, 111453. https://doi.org/10.1016/j.compstruct.2019.111453.

Liu, C., Deng, F., Heng, Q., Cai, X., Zhu, R. and Liserre, M. (2020a), "Crossing thyristor branches based hybrid modular multilevel converters for DC line faults", *IEEE T Ind. Electron.*, **68**(10). https://doi.org/10.1109/TIE.2020.3026277.

Liu, Z., Su, S., Xi, D. and Habibi, M. (2020b), "Vibrational responses of a MHC viscoelastic thick annular plate in thermal environment using GDQ method", *Mech. Based Des. Struct.*, 1-26. https://doi.org/10.1080/15397734.2020.1784201.

Liu, Z., Wu, X., Yu, M. and Habibi, M. (2020c), "Large-amplitude dynamical behavior of multilayer graphene platelets reinforced nanocomposite annular plate under thermo-mechanical loadings", *Mech. Based Des. Struct.*, 1-25. https://doi.org/10.1080/15397734.2020.1815544.

Liu, H., Zhao, Y., Pishbin, M., Habibi, M., Bashir, M. and Issakhov, A. (2021a), "A comprehensive mathematical simulation of the composite size-dependent rotary 3D micro-system via two-dimensional generalized differential quadrature method", *Eng. Comput.*, 1-16. https://doi.org/10.1007/s00366-021-01419-2.

Liu, Y., Wang, W., He, T., Moradi, Z. and Larco Benítez, M.A. (2021b), "On the modelling of the vibration behaviors via discrete singular convolution method for a high-order sector annular system", *Eng. Comput.*, 1-23. https://doi.org/10.1007/s00366-021-01454-z.

Ma, L., Liu, X. and Moradi, Z. (2021a), "On the chaotic behavior of graphene-reinforced annular systems under harmonic excitation", *Eng. Comput.*,1-25. https://doi.org/10.1007/s00366-020-01210-9.

Ma, R., Karimzadeh, M., Ghabussi, A., Zandi, Y., Baharom, S., Selmi, A. and Maureira-Carsalade, N. (2021b), "Assessment of composite beam performance using GWO–ELM metaheuristic algorithm", *Eng. Comput.*, 1-17. https://doi.org/10.1007/s00366-021-01363-1.

Medani, M., Benahmed, A., Zidour, M., Heireche, H., Tounsi, A., Bousahla, A.A., Tounsi, A. and Mahmoud, S. (2019), "Static and dynamic behavior of (FG-CNT) reinforced porous sandwich plate using energy principle", *Steel Compos. Struct.*, **32**(5), 595-610. https://doi.org/10.12989/scs.2019.32.5.595.

Mi, C., Huang, Y., Fu, C., Zhang, Z. and Postolache, O. (2021), "Vision-based measurement: Actualities and developing trends in automated container terminals", *IEEE Instru. Meas. Mag.*, **24**(4), 65-76. https://doi.org/10.1109/MIM.2021.9448257.

Moayedi, H., Habibi, M., Safarpour, H., Safarpour, M. and Foong, L. (2019), "Buckling and frequency responses of a graphene nanoplatelet reinforced composite microdisk", *Int. J. Appl. Mech.*, **11**(10), 1950102. https://doi.org/10.1142/S1758825119501023.

Moayedi, H., Aliakbarlou, H., Jebeli, M., Noormohammadiarani, O., Habibi, M., Safarpour, H. and Foong, L. (2020a), "Thermal buckling responses of a graphene reinforced composite micropanel structure", *Int. J. Appl. Mech.*, **12**(1), 2050010. https://doi.org/10.1142/S1758825120500106.

Moayedi, H., Darabi, R., Ghabussi, A., Habibi, M. and Foong, L.K. (2020b), "Weld orientation effects on the formability of tailor welded thin steel sheets", *Thin Wall. Struct.*, **149**, 106669. https://doi.org/10.1016/j.tws.2020.106669.

Moayedi, H., Ebrahimi, F., Habibi, M., Safarpour, H. and Foong, L.K. (2020c), "Application of nonlocal strain–stress gradient theory and GDQEM for thermo-vibration responses of a laminated composite nanoshell", *Eng. Comput.*, 1-16. https://doi.org/10.1007/s00366-020-01002-1.

Mohammadgholiha, M., Shokrgozar, A., Habibi, M. and Safarpour, H. (2019), "Buckling and frequency analysis of the nonlocal strain–stress gradient shell reinforced with graphene nanoplatelets", *J. Vib. Control*, **25**(19-20), 2627-2640. https://doi.org/10.1177/1077546319863251.

Mohammadi, A., Lashini, H., Habibi, M. and Safarpour, H. (2019), "Influence of viscoelastic foundation on dynamic behaviour of the double walled cylindrical inhomogeneous micro shell using MCST and with the aid of GDQM", *J. Solid Mech.*, **11**(2), 440-453. https://doi.org/10.22034/JSM.2019.665264.

Moradi, Z., Davoudi, M., Ebrahimi, F. and Ehyaei, A.F. (2021), "Intelligent wave dispersion control of an inhomogeneous micro-shell using a proportional-derivative smart controller", *Wave. Random Complex*, 1-24. https://doi.org/10.1080/17455030.2021.1926572.

Morasaei, A., Ghabussi, A., Aghlmand, S., Yazdani, M., Baharom, S. and Assilzadeh, H. (2021), "Simulation of steel–concrete composite floor system behavior at elevated temperatures via multi-hybrid metaheuristic framework", *Eng. Comput.*, 1-16. https://doi.org/10.1007/s00366-020-01228-z.

Mou, B., Bai, Y. and Patel, V. (2020), "Post-local buckling failure of slender and over-design circular CFT columns with high-strength materials", *Eng. Struct.*, **210**, 110197. https://doi.org/10.1016/j.engstruct.2020.110197.

Mukhopadhyay, T. and Adhikari, S. (2016), "Free-vibration analysis of sandwich panels with randomly irregular honeycomb core", *J. Eng. Mech.*, **142**(11), 06016008. https://doi.org/10.1061/(ASCE)EM.1943-7889.0001153

Ni, T., Liu, D., Xu, Q., Huang, Z., Liang, H. and Yan, A. (2020a), "Architecture of cobweb-based redundant TSV for clustered faults", *IEEE T Very Large Scale Integration (VLSI) Syst.*, **28**(7), 1736-1739. https://doi.org/10.1109/TVLSI.2020.2995094.

Ni, T., Yang, Z., Chang, H., Zhang, X., Lu, L., Yan, A., Huang, Z. and Wen, X. (2020b), "A novel TDMA-based fault tolerance technique for the TSVs in 3D-ICs using honeycomb topology", *IEEE T Emerg. Topic Comput.*, **9**(2), 724-734. https://doi.org/10.1109/TETC.2020.2969237

Oyarhossein, M.A., Alizadeh, A.A., Habibi, M., Makkiabadi, M., Daman, M., Safarpour, H. and Jung, D.W. (2020), "Dynamic response of the nonlocal strain-stress gradient in laminated polymer composites microtubes", *Sci. Rep.*, **10**(1), 1-19. https://doi.org/10.1038/s41598-020-61855-w.

Peng, D., Chen, S., Darabi, R., Ghabussi, A. and Habibi, M. (2021), "Prediction of the bending and out-of-plane loading effects on formability response of the steel sheets", *Arch. Civil Mech. Eng.*, **21**(2), 74. https://doi.org/10.1007/s43452-021-00227-1.

Pourjabari, A., Hajilak, Z.E., Mohammadi, A., Habibi, M. and Safarpour, H. (2019), "Effect of porosity on free and forced vibration characteristics of the GPL reinforcement composite nanostructures", *Comput. Math. Appl.*, **77**(10), 2608-2626. https://doi.org/10.1016/j.camwa.2018.12.041.

Rabhi, M., Benrahou, K.H., Kaci, A., Houari, M.S.A., Bourada, F., Bousahla, A.A., Tounsi, A., Bedia, E.A., Mahmoud, S. and Tounsi, A. (2020), "A new innovative 3-unknowns HSDT for buckling and free vibration of exponentially graded sandwich plates resting on elastic foundations under various boundary conditions", *Geomech. Eng.*, **22**(2), 119-132. https://doi.org/10.12989/gae.2020.22.2.119.

Reddy, J.N. (2003), *Mechanics of Laminated Composite Plates and Shells: Theory and Analysis*, CRC press.

SafarPour, H. and Ghadiri, M. (2017), "Critical rotational speed, critical velocity of fluid flow and free vibration analysis of a spinning SWCNT conveying viscous fluid", *Microfluid. Nanofluid.*, **21**(2), 22. https://doi.org/10.1007/s10404-017-1858-y.

Safarpour, H., Hosseini, M. and Ghadiri, M. (2017a), "Influence of three-parameter viscoelastic medium on vibration behavior of a cylindrical nonhomogeneous microshell in thermal environment: An exact solution", *J. Therm. Stress.*, **40**(11), 1353-1367. https://doi.org/10.1080/01495739.2017.1350827.

Safarpour, H., Mohammadi, K., Ghadiri, M. and Rajabpour, A.

(2017b), "Influence of various temperature distributions on critical speed and vibrational characteristics of rotating cylindrical microshells with modified lengthscale parameter", *Eur. Phys. J. Plus*, **132**(6), 1-19. https://doi.org/10.1140/epjp/i2017-11551-4.

Safarpour, H., Ghanizadeh, S.A. and Habibi, M. (2018), "Wave propagation characteristics of a cylindrical laminated composite nanoshell in thermal environment based on the nonlocal strain gradient theory", *Eur. Phys. J. Plus*, **133**(12), 532. https://doi.org/10.1140/epjp/i2018-12385-2.

Safarpour, H., Hajilak, Z.E. and Habibi, M. (2019a), "A size-dependent exact theory for thermal buckling, free and forced vibration analysis of temperature dependent FG multilayer GPLRC composite nanostructures restring on elastic foundation", *Int. J. Mech. Mater. Des.*, **15**(3), 569-583. https://doi.org/10.1007/s10999-018-9431-8.

Safarpour, H., Pourghader, J. and Habibi, M. (2019b), "Influence of spring-mass systems on frequency behavior and critical voltage of a high-speed rotating cantilever cylindrical three-dimensional shell coupled with piezoelectric actuator", *J. Vib. Control*, **25**(9), 1543-1557. https://doi.org/10.1177/1077546319828465.

Safarpour, M., Ebrahimi, F., Habibi, M. and Safarpour, H. (2020a), "On the nonlinear dynamics of a multi-scale hybrid nanocomposite disk", *Eng. Comput.*, **37**(3), 2369-2388. https://doi.org/10.1007/s00366-020-00949-5.

Safarpour, M., Ghabussi, A., Ebrahimi, F., Habibi, M. and Safarpour, H. (2020b), "Frequency characteristics of FG-GPLRC viscoelastic thick annular plate with the aid of GDQM", *Thin Wall. Struct.*, **150**, 106683. https://doi.org/10.1016/j.tws.2020.106683.

Shahverdi, H., Barati, M.R. and Hakimelahi, B. (2019), "Post-buckling analysis of honeycomb core sandwich panels with geometrical imperfection and graphene reinforced nano-composite face sheets", *Mater. Res. Express*, **6**(9), 095017. https://doi.org/10.1088/2053-1591/ab2b74/meta.

Shao, Y., Zhao, Y., Gao, J. and Habibi, M. (2021), "Energy absorption of the strengthened viscoelastic multi-curved composite panel under friction force", *Arch. Civil Mech. Eng.*, **21**(4), 1-29. https://doi.org/10.1007/s43452-021-00279-3.

Shariati, M., Sulong, N.R. and Khanouki, M.A. (2012), "Experimental assessment of channel shear connectors under monotonic and fully reversed cyclic loading in high strength concrete", *Mater. Des.*, **34**, 325-331. https://doi.org/10.1016/j.matdes.2011.08.008.

Shariati, M., Sulong, N.R., Shariati, A. and Khanouki, M.A. (2016a), "Behavior of V-shaped angle shear connectors: experimental and parametric study", *Mater. Struct.*, **49**(9), 3909-3926. https://doi.org/10.1617/s11527-015-0762-8.

Shariati, M., Sulong, N.R., Shariati, A. and Kueh, A. (2016b), "Comparative performance of channel and angle shear connectors in high strength concrete composites: An experimental study", *Constr. Build. Mater.*, **120**, 382-392. https://doi.org/10.1016/j.conbuildmat.2016.05.102.

Shariati, M., Faegh, S.S., Mehrabi, P., Bahavarnia, S., Zandi, Y., Masoom, D.R., Toghroli, A., Trung, N.-T. and Salih, M.N. (2019), "Numerical study on the structural performance of corrugated low yield point steel plate shear walls with circular openings", *Steel Compos. Struct.*, **33**(4), 569-581. https://doi.org/10.12989/scs.2019.33.4.569.

Shariati, A., Ghabussi, A., Habibi, M., Safarpour, H., Safarpour, M., Tounsi, A. and Safa, M. (2020a), "Extremely large oscillation and nonlinear frequency of a multi-scale hybrid disk resting on nonlinear elastic foundation", *Thin Wall. Struct.*, **154**, 106840. https://doi.org/10.1016/j.tws.2020.106840.

Shariati, A., Habibi, M., Tounsi, A., Safarpour, H. and Safa, M. (2020b), "Application of exact continuum size-dependent theory for stability and frequency analysis of a curved cantilevered microtubule by considering viscoelastic properties", *Eng. Comput.*, 1-20. https://doi.org/10.1007/s00366-020-01024-9.

Shariati, A., Mohammad-Sedighi, H., Żur, K.K., Habibi, M. and Safa, M. (2020c), "On the vibrations and stability of moving viscoelastic axially functionally graded nanobeams", *Materials*, **13**(7), 1707. https://doi.org/10.3390/ma13071707.

Shariati, M., Azar, S.M., Arjomand, M.-A., Tehrani, H.S., Daei, M. and Safa, M. (2020d), "Evaluating the impacts of using piles and geosynthetics in reducing the settlement of fine-grained soils under static load", *Geomech. Eng.*, **20**(2), 87-101. https://doi.org/10.12989/gae.2020.20.2.087.

Shariati, M., Ghorbani, M., Naghipour, M., Alinejad, N. and Toghroli, A. (2020e), "The effect of RBS connection on energy absorption in tall buildings with braced tube frame system", *Steel Compos. Struct.*, **34**(3), 393-407. https://doi.org/10.12989/scs.2020.34.3.393.

Shariati, M., Lagzian, M., Maleki, S., Shariati, A. and Trung, N.T. (2020f), "Evaluation of seismic performance factors for tension-only braced frames", *Steel Compos. Struct.*, **35**(4), 599-609. https://doi.org/10.12989/scs.2020.35.4.599.

Shariati, M., Mafipour, M.S., Ghahremani, B., Azarhomayun, F., Ahmadi, M., Trung, N.T. and Shariati, A. (2020g), "A novel hybrid extreme learning machine–grey wolf optimizer (ELM-GWO) model to predict compressive strength of concrete with partial replacements for cement", *Eng. Comput.*, 1-23. https://doi.org/10.1007/s00366-020-01081-0.

Shariati, M., Mafipour, M.S., Mehrabi, P., Ahmadi, M., Wakil, K., Trung, N.T. and Toghroli, A. (2020h), "Prediction of concrete strength in presence of furnace slag and fly ash using Hybrid ANN-GA (Artificial Neural Network-Genetic Algorithm)", *Smart Struct. Syst.*, **25**(2), 183-195. https://doi.org/10.12989/sss.2020.25.2.183.

Shariati, M., Naghipour, M., Yousofizinsaz, G., Toghroli, A. and Tabarestani, N.P. (2020i), "Numerical study on the axial compressive behavior of built-up CFT columns considering different welding lines", *Steel Compos. Struct.* **34**(3), 377-391, http://doi.org/10.12989/scs.2020.34.3.377.

Shariati, M., Tahmasbi, F., Mehrabi, P., Bahadori, A. and Toghroli, A. (2020j), "Monotonic behavior of C and L shaped angle shear connectors within steel-concrete composite beams: an experimental investigation", *Steel Compos Struct.* **35**(2), 237-247. http://doi.org/10.12989/scs.2020.35.2.237.

Shariati, M., Davoodnabi, S.M., Toghroli, A., Kong, Z. and Shariati, A. (2021a), "Hybridization of metaheuristic algorithms with adaptive neuro-fuzzy inference system to predict load-slip behavior of angle shear connectors at elevated temperatures", *Compos. Struct.*, **278**, 114524. https://doi.org/10.1016/j.compstruct.2021.114524.

Shariati, M., Shariati, A., Trung, N.T., Shoaei, P., Ameri, F., Bahrami, N. and Zamanabadi, S.N. (2021b), "Alkali-activated slag (AAS) paste: Correlation between durability and microstructural characteristics", *Constr. Build. Mater.*, **267**, 120886. https://doi.org/10.1016/j.conbuildmat.2020.120886.

Shokrgozar, A., Ghabussi, A., Ebrahimi, F., Habibi, M. and Safarpour, H. (2020), "Viscoelastic dynamics and static responses of a graphene nanoplatelets-reinforced composite cylindrical microshell", *Mech. Based Des. Struct.*, 1-28. https://doi.org/10.1080/15397734.2020.1719509.

Shokrgozar, A., Safarpour, H. and Habibi, M. (2020), "Influence of system parameters on buckling and frequency analysis of a spinning cantilever cylindrical 3D shell coupled with piezoelectric actuator", *Proceedings of the Institution of Mechanical Engineers, Part C: Journal of Mechanical Engineering Science*, **234**(2), 512-529. https://doi.org/10.1177/0954406219883312.

Shu, C. (2012), *Differential Quadrature and Its Application in*

Engineering, Springer Science & Business Media.

Shu, C. and Richards, B.E. (1992), "Application of generalized differential quadrature to solve two-dimensional incompressible Navier-Stokes equations", *Int. J. Numer. Meth. Fl.*, **15**(7), 791-798. https://doi.org/10.1002/fld.1650150704.

Sobhy, M. (2020), "Differential quadrature method for magneto-hygrothermal bending of functionally graded graphene/Al sandwich-curved beams with honeycomb core via a new higher-order theory", *J. Sandw. Struct. Mater.*, **23**(5), 1662-1700. https://doi.org/10.1177/1099636219900668.

Suryawanshi, V.J., Pawar, A.C., Palekar, S.P. and Rade, K.A. (2020), "Defect detection of composite honeycomb structure by vibration analysis technique", *Mater. Today Proceedings*, **27**, 2731-2735. https://doi.org/10.1016/j.matpr.2019.12.192.

Tran, T.T., Tran, V.K., Le, P.B., Phung, V.M., Do, V.T. and Nguyen, H.N. (2020), "Forced vibration analysis of laminated composite shells reinforced with graphene nanoplatelets using finite element method", *Adv. Civil Eng.*, 1471037. https://doi.org/10.1155/2020/1471037.

Wang, Y.J., Zhang, Z.J., Xue, X.M. and Zhang, L. (2019), "Free vibration analysis of composite sandwich panels with hierarchical honeycomb sandwich core", *Thin Wall. Struct.*, **145**, 106425. https://doi.org/10.1016/j.tws.2019.106425.

Wang, Y., Zeng, R. and Safarpour, M. (2020a), "Vibration analysis of FG-GPLRC annular plate in a thermal environment", *Mech. Based Des. Struct.*, 1-19. https://doi.org/10.1080/15397734.2020.1719508.

Wang, Z., Yu, S., Xiao, Z. and Habibi, M. (2020b), "Frequency and buckling responses of a high-speed rotating fiber metal laminated cantilevered microdisk", *Mech. Adv. Mater. Struct.*, 1-14. https://doi.org/10.1080/15376494.2020.1824284.

Wang, H., Zhang, H., Dousti, R. and Safarpour, H. (2021), "Dynamic simulation of moderately thick annular system coupled with shape memory alloy and multi-phase nanocomposite face sheets", *Eng. Comput.*, 1-24. https://doi.org/10.1007/s00366-020-01246-x.

Weng, L., He, Y., Peng, J., Zheng, J. and Li, X. (2021), "Deep cascading network architecture for robust automatic modulation classification", *Neurocomputing*, **455**, 308-324. https://doi.org/10.1016/j.neucom.2021.05.010

Wu, H., Zhu, J., Kitipornchai, S., Wang, Q., Ke, L.L. and Yang, J. (2020), "Large amplitude vibration of functionally graded graphene nanocomposite annular plates in thermal environments", *Compos. Struct.*, **239**, 112047. https://doi.org/10.1016/j.compstruct.2020.112047.

Wu, J. and Habibi, M. (2021), "Dynamic simulation of the ultra-fast-rotating sandwich cantilever disk via finite element and semi-numerical methods", *Eng. Comput.*, 1-17. https://doi.org/10.1007/s00366-021-01396-6.

Wu, W. (2021), "Adaptive momentum-based optimization to train deep neural network for computer simulation of hygro-thermo-mechanical vibration performance of laminated plates", *Mech. Based Des. Struct.*, 1-24. https://doi.org/10.1080/15397734.2021.1883442.

Xu, G.D., Zeng, T., Cheng, S., Wang, X.H. and Zhang, K. (2019), "Free vibration of composite sandwich beam with graded corrugated lattice core", *Compos. Struct.*, **229**, 111466. https://doi.org/10.1016/j.compstruct.2019.111466.

Xu, W., Pan, G., Moradi, Z. and Shafiei, N. (2021), "Nonlinear forced vibration analysis of functionally graded non-uniform cylindrical microbeams applying the semi-analytical solution", *Compos. Struct.*, 114395. https://doi.org/10.1016/j.compstruct.2021.114395.

Yu, X., Maalla, A. and Moradi, Z. (2022), "Electroelastic high-order computational continuum strategy for critical voltage and frequency of piezoelectric NEMS via modified multi-physical couple stress theory", *Mech. Syst. Signal Proc.*, **165**, 108373. https://doi.org/10.1016/j.ymssp.2021.108373.

Zhang, Z.J., Han, B., Zhang, Q.C. and Jin, F. (2017), "Free vibration analysis of sandwich beams with honeycomb-corrugation hybrid cores", *Compos. Struct.*, **171**, 335-344. https://doi.org/10.1016/j.compstruct.2017.03.045.

Zhang, X., Wang, Y., Wang, C., Su, C.Y., Li, Z. and Chen, X. (2018), "Adaptive estimated inverse output-feedback quantized control for piezoelectric positioning stage", *IEEE T Cybernet.*, **49**(6), 2106-2118. https://doi.org/10.1109/TCYB.2018.2826519.

Zhang, Y. and Li, Y. (2019), "Nonlinear dynamic analysis of a double curvature honeycomb sandwich shell with simply supported boundaries by the homotopy analysis method", *Compos. Struct.*, **221**, 110884. https://doi.org/10.1016/j.compstruct.2019.04.056.

Zhang, L., Zheng, H., Wan, T., Shi, D., Lyu, L. and Cai, G. (2021a), "An integrated control algorithm of power distribution for islanded microgrid based on improved virtual synchronous generator", *IET Renew. Power Gener.*, **15**(12),2674-2685. https://doi.org/10.1109/TSG.2016.2521405

Zhang, W., Liu, Z., Liang, Z., Oslub, K. and Safarpour, H. (2021b), "A comprehensive computer simulation of the size-dependent sector or complete microsystem via two-dimensional generalized differential quadrature method", *Eng. Comput.*, 1-17. https://doi.org/10.1007/s00366-021-01440-5.

Zhang, Y., Wang, Z., Tazeddinova, D., Ebrahimi, F., Habibi, M. and Safarpour, H. (2021c), "Enhancing active vibration control performances in a smart rotary sandwich thick nanostructure conveying viscous fluid flow by a PD controller", *Wave. Random Complex*, 1-24. https://doi.org/10.1080/17455030.2021.1948627.

Zhao, H., Wang, L., Issakhov, A. and Safarpour, H. (2021a), "Poroelasticity framework for stress/strain responses of the multi-phase circular/annular systems resting on various types of elastic foundations", *Eur. Phys. J. Plus*, **136**(8), 1-44. https://doi.org/10.1140/epjp/s13360-021-01761-w.

Zhao, Y., Moradi, Z., Davoudi, M. and Zhuang, J. (2021b), "Bending and stress responses of the hybrid axisymmetric system via state-space method and 3D-elasticity theory", *Eng. Comput.*, 1-23. https://doi.org/10.1007/s00366-020-01242-1.

Zhou, C., Zhao, Y., Zhang, J., Fang, Y. and Habibi, M. (2020), "Vibrational characteristics of multi-phase nanocomposite reinforced circular/annular system", *Adv. Nano Res.*, **9**(4), 295-307. https://doi.org/10.12989/anr.2020.9.4.295.

Zine, A., Bousahla, A.A., Bourada, F., Benrahou, K.H., Tounsi, A., Adda Bedia, E., Mahmoud, S. and Tounsi, A. (2020), "Bending analysis of functionally graded porous plates via a refined shear deformation theory", *Comput. Concrete*, **26**(1), 63-74, http://doi.org/10.12989/cac.2020.26.1.063.

CC